

POHL, F., GERMANN, A.L., MAO, J., HOU, S., BAKARE, B., KONG THOO LIN, P., YATES, K., NONET, M.L., AKK, G., KORNFELD, K. and HELD, J.M. 2023. UNC-49 is a redox-sensitive GABAA receptor that regulates the mitochondrial unfolded protein response cell nonautonomously. *Science advances* [online], 9(44). Available from: <https://doi.org/10.1126/sciadv.adh2584>

UNC-49 is a redox-sensitive GABAA receptor that regulates the mitochondrial unfolded protein response cell nonautonomously.

POHL, F., GERMANN, A.L., MAO, J., HOU, S., BAKARE, B., KONG THOO LIN, P., YATES, K., NONET, M.L., AKK, G., KORNFELD, K. and HELD, J.M.

2023



BIOCHEMISTRY

UNC-49 is a redox-sensitive GABA_A receptor that regulates the mitochondrial unfolded protein response cell nonautonomously

Franziska Pohl^{1,2}, Allison L. Germann³, Jack Mao¹, Sydney Hou², Bayode Bakare⁴, Paul Kong Thoo Lin⁴, Kyari Yates⁴, Michael L. Nonet⁵, Gustav Akk^{3,6}, Kerry Kornfeld², Jason M. Held^{1,3,7*}

The γ -aminobutyric acid–mediated (GABAergic) system participates in many aspects of organismal physiology and disease, including proteostasis, neuronal dysfunction, and life-span extension. Many of these phenotypes are also regulated by reactive oxygen species (ROS), but the redox mechanisms linking the GABAergic system to these phenotypes are not well defined. Here, we report that GABAergic redox signaling cell nonautonomously activates many stress response pathways in *Caenorhabditis elegans* and enhances vulnerability to proteostasis disease in the absence of oxidative stress. Cell nonautonomous redox activation of the mitochondrial unfolded protein response (mitoUPR) proteostasis network requires UNC-49, a GABA_A receptor that we show is activated by hydrogen peroxide. MitoUPR induction by a spinocerebellar ataxia type 3 (SCA3) *C. elegans* neurodegenerative disease model was similarly dependent on UNC-49 in *C. elegans*. These results demonstrate a multi-tissue paradigm for redox signaling in the GABAergic system that is transduced via a GABA_A receptor to function in cell nonautonomous regulation of health, proteostasis, and disease.

INTRODUCTION

Reactive oxygen species (ROS) and redox biology play multifaceted roles in health and disease and are needed for cellular signaling, homeostasis, and communication in a wide range of cell types and organisms (1, 2). In *Caenorhabditis elegans*, redox biology plays a functional role in reproduction (3), cuticle structure (4), behavior/environmental sensing (5), and life span (6).

However, important questions in redox biology remain unanswered, especially molecular understanding of the redox signaling that coordinates biological processes and phenotypes across tissues. This is because characterizing tissue-specific redox biology and chemistry in an organismal environment is especially challenging (6–8). First, exogenous oxidants and pro-oxidants (e.g., H₂O₂, juglone, rotenone, and paraquat) cannot be applied to specific tissues. Second, mutants that have altered redox biology are rarely characterized in a tissue-specific manner. Furthermore, the mitochondrial mutants that display increased mitochondrial ROS and are commonly used (e.g., *nuo-6*, *isp-1*, and *clk-1*) (9, 10) also display additional phenotypes such as altered mitochondrial metabolism that limit clear understanding of redox biology (8, 11). Last, the diverse chemical kinetics, reactivity, and diffusibility of each ROS (e.g., hydrogen peroxide, superoxide, hydroxyl radical, and singlet oxygen) can define redox signaling networks (1), but these factors are less explored in multicellular organisms where additional

layers of regulation may be present. For example, while charged radicals such as superoxide (O₂^{•-}) cannot traverse cell membranes, hydrogen peroxide (H₂O₂) is a diffusible second messenger with the potential to act cell nonautonomously (12, 13).

Tissue-specific investigation of redox biology has recently become possible via ROS-producing optogenetic proteins such as KillerRed and Supernova (13–15). These optogenetic proteins have been widely used in *C. elegans* because these animals are optically transparent and tissue-specific promoters are widely available. However, most studies using this technology have focused on oxidative stress to ablate specific cells (15, 16), generate organelle damage, or inactivate specific proteins (17, 18).

C. elegans is ideal for in vivo analysis of redox signaling in specific tissues due to the wide array of behaviors and phenotypes that can be assayed (19, 20). We focused on investigating neuronal redox biology, which is especially dynamic since ROS can be produced in neurons by axonal firing (21), hypoxia (22), altered metabolism (23, 24), and aging (25). ROS are also capable of regulating neuronal processes such as synaptic transmission and plasticity (26, 27). We focused on the γ -aminobutyric acid–mediated (GABAergic) system since mitochondrial ROS has been implicated in strengthening GABA-mediated synaptic transmission (23) and the GABAergic system regulates many processes and organismal phenotypes associated with altered ROS and redox biology, including neurodegeneration (28), proteostasis and protein folding (29, 30), life-span extension (31), and immunity (32). However, while GABA_A receptors can be oxidized, it is unclear how their redox regulation is mechanistically linked to these diverse phenotypes (23, 33–35).

Here, we developed an optogenetic platform that enables long-term production of ROS across a full continuum of levels ranging from redox signaling to oxidative stress in many *C. elegans* individuals simultaneously. We applied this platform to control and sustain ROS production in GABAergic neurons using worms that express

¹Department of Medicine, Washington University School of Medicine, St. Louis, MO, USA. ²Department of Developmental Biology, Washington University School of Medicine, St. Louis, MO, USA. ³Department of Anesthesiology, Washington University School of Medicine, St. Louis, MO, USA. ⁴School of Pharmacy and Life Sciences, Robert Gordon University, Aberdeen, UK. ⁵Department of Neuroscience, Washington University School of Medicine, St. Louis, MO, USA. ⁶Taylor Family Institute for Innovative Psychiatric Research, Washington University School of Medicine, St. Louis, MO, USA. ⁷Siteman Cancer Center, Washington University School of Medicine, St. Louis, MO, USA.

*Corresponding author. Email: jheld@wustl.edu

Copyright © 2023 The Authors, some rights reserved; exclusive licensee American Association for the Advancement of Science. No claim to original U.S. Government Works. Distributed under a Creative Commons Attribution NonCommercial License 4.0 (CC BY-NC).

KillerRed under the vesicular GABA transporter (*unc-47*) promoter. In parallel, we assayed a spinocerebellar ataxia type 3 (SCA3) *C. elegans* neurodegenerative disease model that is associated with increased ROS and proteostasis failure (36, 37). The mitochondrial unfolded protein response (mitoUPR) is cell nonautonomously activated in both strains in a ROS-dependent manner, and this induction required the GABA_A receptor UNC-49, which is primarily expressed in neurons (GABAergic, cholinergic, and interneurons) and muscle cells (38–40). Using electrophysiology, we determined that H₂O₂ increases UNC-49B channel activity independent of GABA and also potentiates the channel activation by GABA. Our results demonstrate a multi-tissue GABAergic redox signaling network that acts via GABA_A receptor oxidation to cell nonautonomously regulate stress response signaling and vulnerability to proteostasis disease.

RESULTS

An LED-based optogenetic platform enables investigation of GABAergic redox signaling and oxidative stress

Investigating GABAergic redox biology requires developing an approach to control and sustain ROS production across a continuum of levels ranging from redox signaling to oxidative stress in many *C. elegans* individuals simultaneously. We used large, white light producing light-emitting diodes (LEDs) controlled by dimmer switches to modulate light intensity (fig. S1, A and B). To optogenetically produce ROS specifically in GABAergic neurons, we used the *C. elegans* strain we term “GABA-KR” (*wpIs15* [*unc-47p*::KillerRed] X; GABA-KR) that expresses KillerRed (KR) in the cytoplasm of GABAergic neurons using the *unc-47* promoter (Fig. 1A) (15). Light activation of KR rapidly damages and permanently inactivates GABAergic neurons, which induces a shrinker phenotype (15). While previous work permanently inactivated neurons using high light intensities (100 to 460 mW/cm²) for a short duration (5 to 120 min) (15), we observed that lower light intensities (0.3 to 3.0 mW/cm²) for longer durations (72 hours) were able to similarly induce neuronal damage in the GABA-KR strain in a light intensity-dependent manner (Fig. 1B).

Since light can induce heat, and temperature can influence many aspects of *C. elegans*’ physiology (41), we routinely measured the temperature of the nematode growth medium (NGM) dishes that worms were cultured on. There was no increase in temperature at ≤1.0 mW/cm² light, but 3.0 mW/cm² light increased the temperature by 1°C (fig. S1C). We additionally verified that environmental conditions were stable using the temperature-sensitive *hsp-16.2p*::GFP reporter strain (42). No increase in *hsp-16.2p*::GFP expression was observed at light conditions ≤1.0 mW/cm², but 3.0 mW/cm² caused a small, but significant, increase in green fluorescent protein (GFP) expression (fig. S1D).

The ROS produced by ≥1.0 mW/cm² light induced phenotypes consistent with oxidative stress. For example, worms exposed to 1.0 or 3.0 mW/cm² displayed abnormal neuronal morphology and fragmentation of neuronal processes including blebbing and pearling as well as smaller and rounder cell bodies (Fig. 1, C and D). These light intensities also decreased the overall size of the GABA-KR worms (Fig. 1E) and altered tissue morphology (Fig. 1C) in a light intensity-dependent manner, which was not observed in wild-type (WT) worms. In contrast, worms exposed to light conditions ≤0.3 mW/cm² displayed no neuronal damage or tissue abnormalities

(Fig. 1C), and the number of animals displaying a shrinker phenotype was only modestly increased (Fig. 1B). To test whether light intensity between 0 and 0.3 mW/cm² affected *C. elegans* health, we measured life span. Light intensities of 0 to 0.3 mW/cm² did not alter life span (Fig. 1F and fig. S1E). These results indicate that this optogenetic platform enables analysis of the full continuum of ROS levels to study redox biology, with ≤0.1 mW/cm² light producing ROS consistent with redox signaling (43, 44) that did not cause detrimental health effects. At the other end of the redox spectrum, light intensities ≥1.0 mW/cm² induced oxidative stress, damaged neuronal morphology and function, and caused detrimental consequences for worm size and tissue morphology.

GABA-KR redox signaling activates diverse stress response pathways cell nonautonomously

We used this optogenetic platform to investigate whether ROS and redox signaling in GABA neurons activates specific stress response pathways at 0 to 3.0 mW/cm² light intensities using four well-characterized GFP reporter strains: *daf-16* (TJ356), *sod-3* (CF1553), *gst-4* (CL2166), and *hsp-6* (SJ4100). DAF-16 is a FoxO transcription factor that mediates stress resistance by translocating from the cytoplasm to the nucleus when activated (45, 46). SOD-3 (superoxide dismutase 3) is a mitochondrial manganese superoxide dismutase that counteracts ROS accumulation by detoxifying superoxide (47). Glutathione S-transferase-4 (GST-4) is a homolog of human sigma GSTs that mitigates oxidative stress by conjugating reduced glutathione (GSH) to electrophiles (48). HSP-6 is the ortholog of human mitochondrial heat shock protein 70 (mthsp70) and a specific mediator of the mitoUPR that regulates proteostasis (49, 50).

Chronic ROS production (72 hours) in GABAergic neurons differentially activated distinct stress responses. For example, *daf16p*::*daf-16a/b*::GFP nuclear translocation was not reliably altered by GABA-KR at the three light intensities evaluated (fig. S2A). However, GFP expression in the three other reporter strains was significantly up-regulated in GABA-KR strains compared to control strains that do not express GABA-KR (Fig. 2, A to C). The *sod-3p*::GFP, *gst-4p*::GFP, and *hsp-6p*::GFP reporters were all very sensitive to ROS in GABAergic neurons and activated by the 0 mW/cm² condition, where light was limited as much as experimentally possible. This is likely because fluorescent proteins such as KR and enhanced GFP (eGFP) produce some ROS even in the absence of light stimulation during chromophore maturation (18, 49, 51). We observed a light-dependent increase in *sod-3p*::GFP expression in the presence of GABA-KR, while *sod-3p*::GFP expression changed minimally in the absence of GABA-KR under all light conditions (Fig. 2A). In contrast, *gst-4p*::GFP expression decreased in the presence of GABA-KR at light intensities corresponding to oxidative stress (Fig. 2B), likely due to oxidative inactivation of this pathway (52).

The *hsp-6p*::GFP reporter of the mitoUPR had the largest fold change by GABA-KR (Fig. 2C), consistent with its known sensitivity to exogenous addition of the ROS generators paraquat, antimycin A, and rotenone (53, 54) and by ROS produced optogenetically in the mitochondrial outer membrane of muscle, intestinal, and neuronal cells (18). In contrast to *sod-3p*::GFP and *gst-4p*::GFP, induction of *hsp-6p*::GFP by GABA-KR was stable at all light intensities.

To determine whether cell nonautonomous activation of stress response pathway was specific to the GABAergic system, we

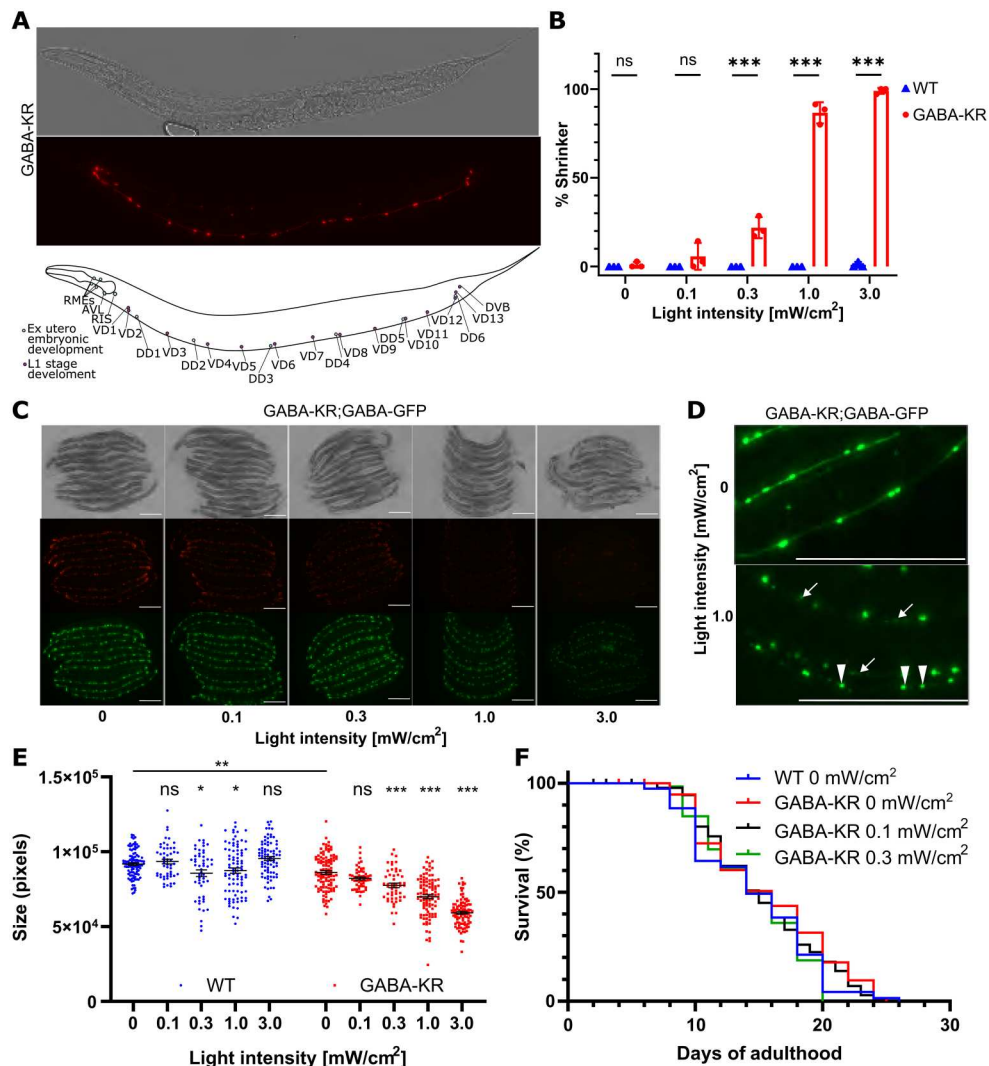


Fig. 1. GABA-KR enables investigation of GABAergic redox signaling and oxidative stress. (A) GABA-KR strain fluorescent image and schematic, indicating GABA-KR expression in GABAergic neurons under *unc-47* promoter. (B) KillerRed activation induces movement defects. Animals were illuminated with LED lights (0 to 3.0 mW/cm²) for 72 hours during development and then scored for the shrinker phenotype caused by GABAergic neuron dysfunction. Three biological replicates, $N \geq 35$ per replicate for KillerRed and WT. Ordinary two-way ANOVA with Šidák's multiple comparison test with a single pooled variance. (C) Brightfield (top) and fluorescent (KR, middle; GFP, bottom) images of the GABAergic neurons of GABA-KR;GABA-GFP (*juls76 [unc-25p::GFP + lin-15(+)] II; wpls15 [unc-47p::KillerRed X]*) animals with 0 to 3.0 mW/cm² illumination. Scale bar, 200 μ m. (D) Enlarged images of 0 (top) and 1.0 mW/cm² (bottom), showing cell body rounding (solid triangle) neuronal process degeneration and blebbing (arrow). Scale bar 200 μ m. (E) Worm size changes induced by GABA-KR, five or more biological replicates, with $N \geq 8$ per replicate. Ordinary two-way ANOVA with Šidák's multiple comparison test, with a single pooled variance to compare WT to GABA-KR and with individual variance computed for each comparison for comparison within strains. (F) Representative life-span curves of GABA-KR worms illuminated with 0 to 0.3 mW/cm² during development (72 hours) compared to WT worms (0 mW/cm²). Kaplan-Meier simple survival analysis with log-rank (Mantel-Cox) test.

crossed the *sod-3p::GFP* and *hsp-6p::GFP* reporter into a strain that expresses KR in cholinergic neurons under the *unc-17* promoter (cholinergic-KR; *wpls14 [unc-17p::KillerRed + unc-122p::GFP]*) (fig. S2B) (15). In contrast to GABA-KR, stimulation with 0 to 3.0 mW/cm² light in the cholinergic-KR strain did not activate *sod-3p::GFP* expression (fig. S2C) or *hsp-6p::GFP* (fig. S2D).

GABA-KR cell nonautonomously activates the mitoUPR proteostasis network

Since the mitoUPR plays a potential role in many disease-relevant processes, we further investigated its activation by GABAergic

redox signaling. First, Western blot analysis confirmed the GABA-KR-dependent increase in *hsp-6p::GFP* expression (Fig. 3A). Image analysis showed that increased *hsp-6p::GFP* expression occurs primarily in the intestine, not the GABAergic neurons where KR is expressed (Fig. 3B). We also observed cell nonautonomous activation of mitoUPR by GABA-KR using the translational reporter for *dve-1 [dve-1p::dve-1::GFP]* (55), a transcription factor that translocates to the nucleus upon mitoUPR activation (Fig. 3C) (55). GABA-KR significantly increased the number of cells with nuclear *dve-1p::dve-1::GFP* (Fig. 3, D and E), primarily in intestinal cells as observed for *hsp-6p::GFP* expression (Figs. 2C

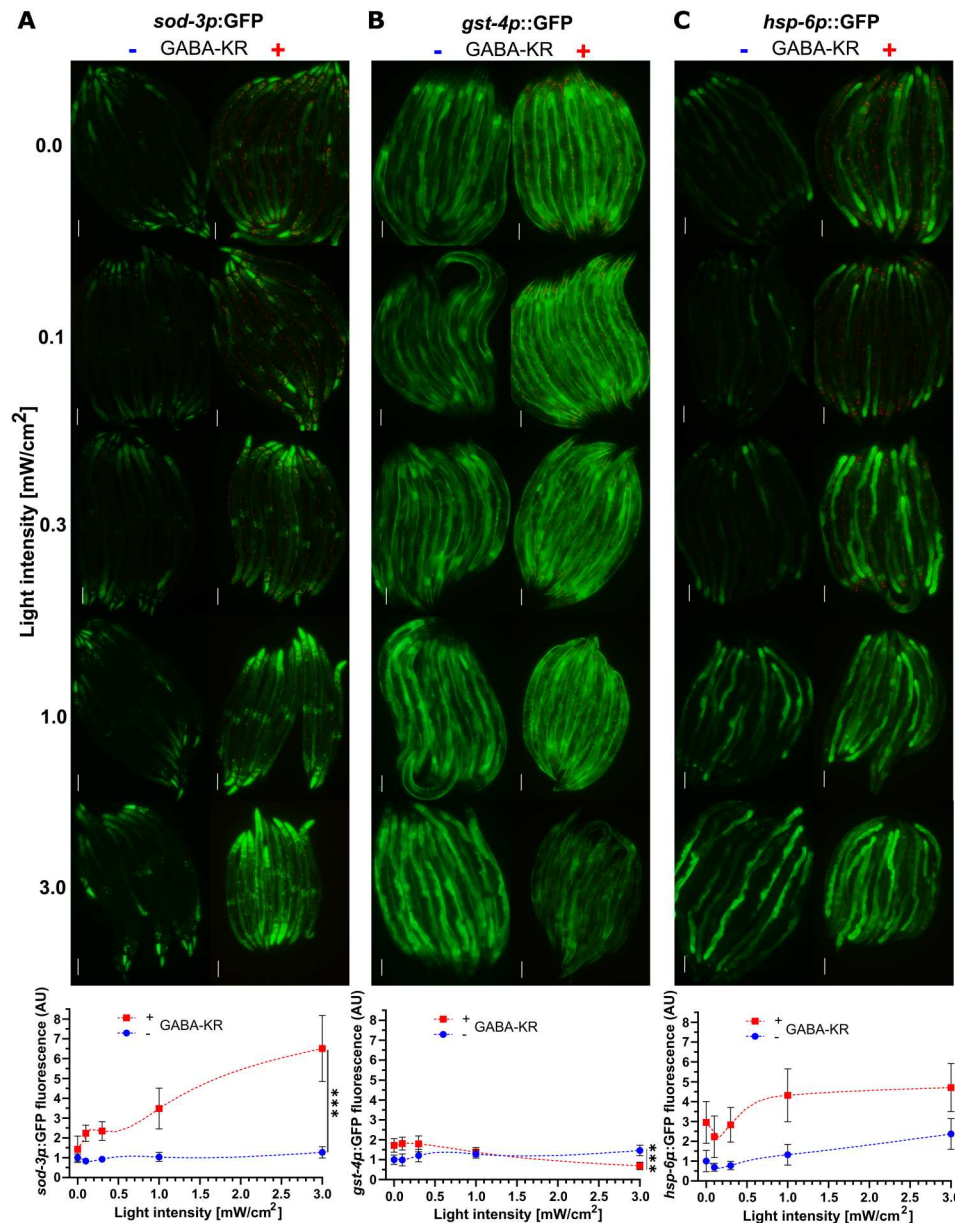


Fig. 2. GABA-KR activates stress response pathways with a diversity of responses. (A) Top: Fluorescent microscope images of multiple *sod-3p::GFP* worms in the absence (left) and presence (right) of GABA-KR between 0 and 3.0 mW/cm². Bottom: GFP intensity measurements of *sod-3p::GFP* in the presence (red, square) and absence (blue, circle) of GABA-KR between 0 and 3.0 mW/cm². (B) Top: Fluorescent microscope images of multiple *gst-4p::GFP* worms in the absence (left) and presence (right) of GABA-KR between 0 and 3.0 mW/cm². Bottom: GFP intensity measurements of *gst-4p::GFP* in the presence (red, square) and absence (blue, circle) of GABA-KR between 0 and 3.0 mW/cm². (C) Top: Fluorescent microscope images of multiple *hsp-6p::GFP* worms in the absence (left) and presence (right) of GABA-KR between 0 and 3.0 mW/cm². Bottom: GFP intensity measurements of *hsp-6p::GFP* in the presence (red, square) and absence (blue, circle) of GABA-KR between 0 and 3.0 mW/cm². All fluorescence intensities were normalized to the respective reporter control at 0 mW/cm² and analyzed using ordinary two-way ANOVA to compare the curves, showing mean \pm SD of three or more biological replicates with $N \geq 6$ for each replicate/condition. Curves created using LOWESS, 10 points in smoothing window. AU, arbitrary units.

and 3B). GABA-KR-dependent DVE-1 nuclear localization was also observed in smaller nuclei in cells close to body wall muscle cells. These results demonstrate that redox signaling in GABAergic neurons is sufficient to activate proteostasis and stress response networks cell nonautonomously.

To determine whether mitoUPR induction depended on the ROS produced by GABA-KR, we treated *hsp-6p::GFP* and GABA-

KR;*hsp-6p::GFP* with *N*-acetylcysteine (NAC), a common antioxidant and U.S. Food and Drug Administration (FDA)-approved drug (56). Treatment of the GABA-KR;*hsp-6p::GFP* strain with 5 mM NAC significantly reduced *hsp-6p::GFP* fluorescence (Fig. 3F), demonstrating that ROS mediate the increased mitoUPR expression caused by GABA-KR. No change was observed in *hsp-6p::GFP* expression following NAC treatment for the control

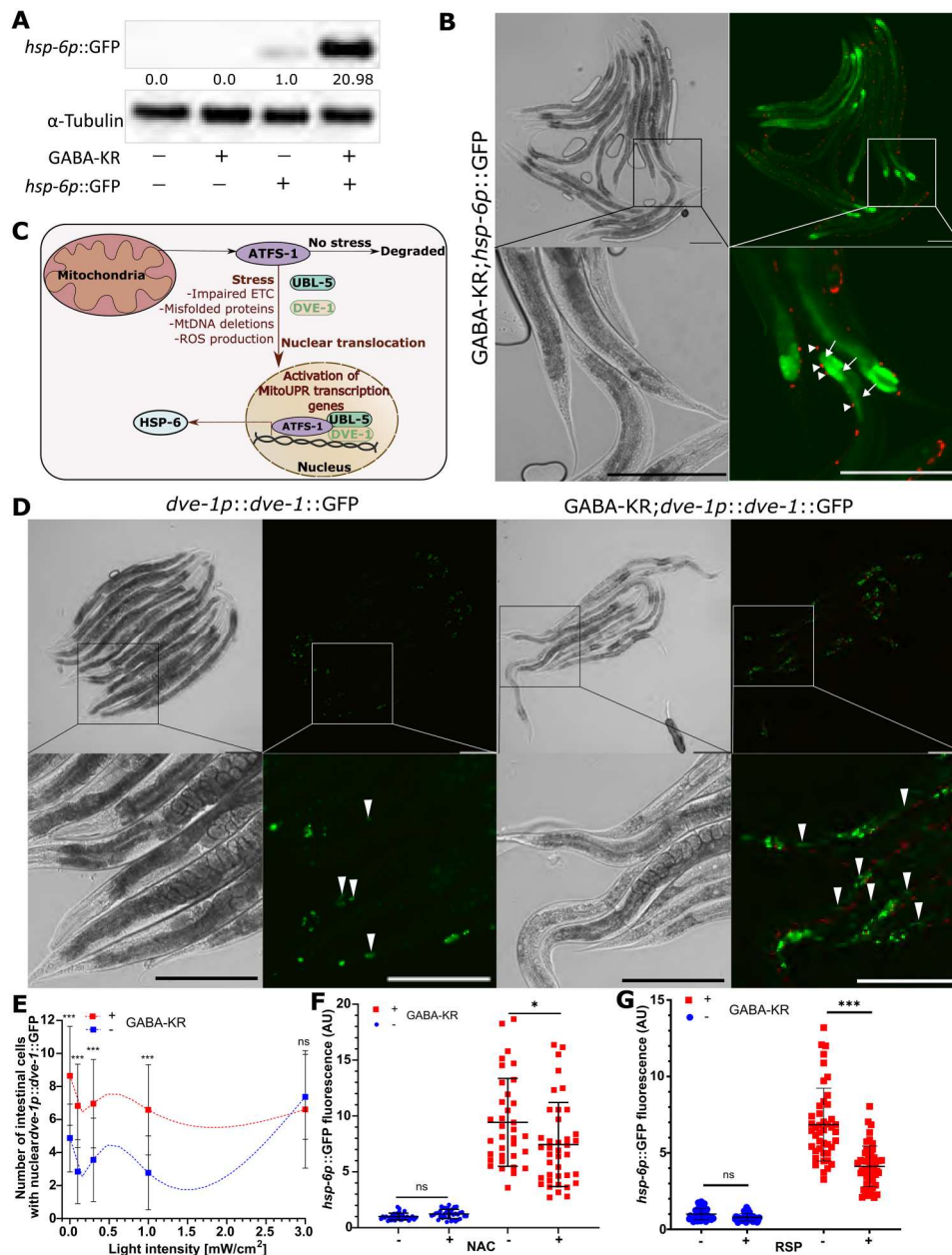


Fig. 3. GABA-KR sufficient to activate mitoUPR cell nonautonomously (ROS dependent). (A) Western blot of *hsp-6p::GFP* in the absence (–) and presence (+) of GABA-KR and respective control strains in the presence (+) and absence (–) of *hsp-6p::GFP*. Values indicate the *hsp-6p::GFP*/α-tubulin ratio changes normalized to the *hsp-6p::GFP* control. (B) Brightfield (left) and fluorescent (right) microscope images of GABA-KR;*hsp-6p::GFP* strains. Top: Full-image 10× magnification. Bottom: Enlarged image highlights cell nonautonomous activation. Arrowheads point at KR in GABAergic neurons, while arrows point at *hsp-6p::GFP* expression in intestines. Scale bar, 200 μm. (C) Schematic of *hsp-6* regulation by *atfs-1* and through *ubl-5* and *dve-1* (89). (D) Brightfield (left) and fluorescent (right) microscope images of *dve-1p::dve-1::GFP* and GABA-KR;*dve-1p::dve-1::GFP* strains. Top: Full-image 10× magnification. Bottom: Enlarged image highlights cell nonautonomous activation. Arrowheads point at intestinal nuclear *dve-1p::dve-1::GFP* expression. Scale bar, 200 μm. (E) Number of intestinal cells with nuclear GFP in *dve-1p::dve-1::GFP* versus *dve-1p::dve-1::GFP*; GABA-KR worms; mean ± SD; ordinary two-way ANOVA and Bonferroni’s multiple comparison test with a single pooled variance. Curves created using LOWESS, 10 points in smoothing window. (F) *hsp-6p::GFP* expression in the presence (+) and absence (–) of GABA-KR and treatment with (+) or without (–) *N*-acetylcysteine (NAC; 5 mM); mean ± SD; ordinary two-way ANOVA and Tukey’s multiple comparison test with a single pooled variance. (G) *hsp-6p::GFP* expression in the presence (+) and absence (–) of GABA-KR and treatment with (+) or without (–) rapeseed pomace (RSP) extract (1 mg/ml); mean ± SD; ordinary two-way ANOVA and Tukey’s multiple comparison test with a single pooled variance.

reporter strain without GABA-KR. To verify this ROS dependence, we also used an extract from rapeseed/canola pomace (RSP extract) that has been shown to have antioxidant activity in vitro (57–59) and in vivo (37). Treatment with the RSP extract also significantly decreased mitoUPR expression of GABA-KR;*hsp-6p::GFP* worms (Fig. 3G). To determine whether *hsp-6p::GFP* fluorescence is increased due to KR-induced ROS production, we used a strain that expresses GFP in GABAergic neurons *oxIs12* [*unc-47p::GFP* + *lin-15(+)*] (60). Due to its structure, GFP is less likely to create ROS than KR (13, 61). Expression of GFP in GABAergic neurons was not sufficient to induce *hsp-6p::GFP* expression (fig. S3). These results demonstrate that ROS produced in GABAergic neurons is required for cell nonautonomous activation of mitoUPR.

The GABA_A receptor UNC-49 is required for activation of the mitoUPR by redox signaling, but GABA synthesis is not

We hypothesized that GABA-KR-dependent activation of the mitoUPR required a canonical component of the *C. elegans* GABAergic system (Fig. 4A). Treatment with exogenous, nontoxic concentrations of GABA was sufficient to increase *hsp-6p::GFP* expression (Fig. 4B and fig. S4A), indicating that GABA neurotransmission was sufficient to activate the mitoUPR. To determine whether the increased mitoUPR expression by GABAergic ROS required endogenous GABA synthesis, we crossed the GABA-KR;*hsp-6p::GFP* strain with an *unc-25(e156)* mutant strain that lacks the sole *C. elegans* glutamic acid decarboxylase enzyme that is required for GABA synthesis (Fig. 4A). Loss of *unc-25* did not decrease, and even increased, *hsp-6p::GFP* by GABA-KR as measured by both imaging (Fig. 4, C and D) and Western blot (Fig. 4G) in the dark and with 0.1 and 0.3 mW/cm² light (fig. S4B). Therefore, GABA synthesis was not required for induction of mitoUPR.

In contrast to GABA synthesis mutants, *unc-49(tm5487)* mutants that lack the GABA_A receptor UNC-49 (39) displayed a significant reduction in *hsp-6p::GFP* expression in the GABA-KR background in the dark (Fig. 4, E to G) and with 0.1 and 0.3 mW/cm² light (fig. S4C). To investigate whether these results were allele specific, since the *unc-49(tm5487)* mutation is a 302-base pair (bp) deletion of *unc-49* covering exons 7 and 8, we used a second *unc-49* mutation, *unc-49(e407)*, which is a nonsense mutation that causes an early stop codon in exon 5. *unc-49(e407)* mutants also displayed significantly reduced *hsp-6p::GFP* expression in the GABA-KR strain in the dark (Fig. 4, H to J) and with 0.1 and 0.3 mW/cm² light (fig. S4D). To determine whether this expression decrease could be due to a decrease in KR expression, we measured KR expression in WT animals as well as *unc-49* mutants. The results show that there is no significant change in KR expression (fig. S4, E and F). To determine whether *unc-49* was required

for the activation of other stress response pathways, we measured *sod-3p::GFP* expression in *unc-49(tm5487)* animals. Expression of *sod-3p::GFP* was increased in *unc-49(tm5487)* mutants (fig. S4G), suggesting that *unc-49* is not required for *sod-3* activation by GABA-KR and may even suppress it. Hence, *unc-49* is required for mitoUPR activation, whereas *unc-25* and GABA synthesis is not required. This suggested that ROS may activate UNC-49 channel activity in a GABA-independent manner.

H₂O₂ increases UNC-49B channel activity

We next sought to determine the molecular mechanism of UNC-49 activation by ROS in GABAergic neurons, which we hypothesized involved redox regulation of the UNC-49 GABA_A receptor itself. Historically, the original studies of *unc-49* reported a single promoter that controls the expression of three UNC-49 protein isoforms (Table 1) (39). Notably, many more UNC-49 isoforms have been detected since, and naming of UNC-49 isoforms in Wormbase (62) is inconsistent with those used in some of the literature. Here, we refer to UNC-49 isoforms using the Wormbase nomenclature and provide Table 1 for clarification. UNC-49C is considered the canonical UNC-49 isoform, but heteromerization with UNC-49F can modulate UNC-49C channel in response to GABA_A receptor-modulating drugs compared to the homomer (38, 39).

We investigated redox activation of UNC-49 using two-electrode voltage clamp electrophysiology in *Xenopus* oocytes. GABA activated both UNC-49B and UNC-49C when expressed individually, demonstrating their functionality as homopentamers (Fig. 5A and fig. S5, A, B, and D).

We next investigated the redox regulation of UNC-49 isoforms. The UNC-49C homomer and the heteromeric UNC-49C/UNC-49F receptors did not respond to treatment with up to 500 μM H₂O₂ (fig. S5, A, B, and D). In contrast, the UNC-49B receptor was directly activated by as little as 30 μM H₂O₂ (Fig. 5, B and C) as observed for the human ρ1 GABA_A receptors (fig. S5C), which was used as positive control. In uninjected *Xenopus laevis* oocytes, exposure to 30 to 500 μM H₂O₂ generated minimal (less than 1.6 nA, total *n* = 5 oocytes) change in holding current, indicating that the responses observed originate from the GABA_A receptor. We next investigated whether H₂O₂ modulated UNC-49B channel activity elicited by GABA and found that H₂O₂ exposure potentiated the response to GABA (Fig. 5D). The normalized potentiation concentration-response curve was fitted with the Hill equation, yielding a fitted maximal response of 3.3 ± 0.6 (best-fit parameter ± SE of the fit; 1 = no effect), an EC₅₀ (median effective concentration) of 311 ± 165 μM, and a Hill coefficient of 1.12 ± 0.34 (Fig. 5E).

These results demonstrate that UNC-49B can be redox-activated, consistent with our model that ROS produced in GABAergic neurons induce mitoUPR and *hsp-6p::GFP* expression via oxidation of UNC-49.

Muscle-specific UNC-49B expression rescues the decrease in mitoUPR activation caused by *unc-49* mutations

UNC-49 is primarily expressed in neurons and muscle cells (fig. S5, E and F) (38–40). During locomotion, the role of UNC-49 in the 19 ventral cord D-type neurons is to inhibit the contraction of body wall muscle cells. Due to the importance of UNC-49 function in muscle cells, we investigated whether reexpression of UNC-49B solely in muscle cells could rescue the decreased *hsp-6p::GFP* expression we observed in *unc-49(e407)* mutants.

Table 1. *C. elegans* UNC-49 isoforms and their naming differences.

Wormbase* (this manuscript)	Previous publications (39)
UNC-49B (T21C12.1b)	UNC-49A
UNC-49C (T21C12.1c)	UNC-49B
UNC-49F (T21C12.1f)	UNC-49C

*https://wormbase.org/species/c_elegans/gene/WBGene00006784#0-9feb1-10.

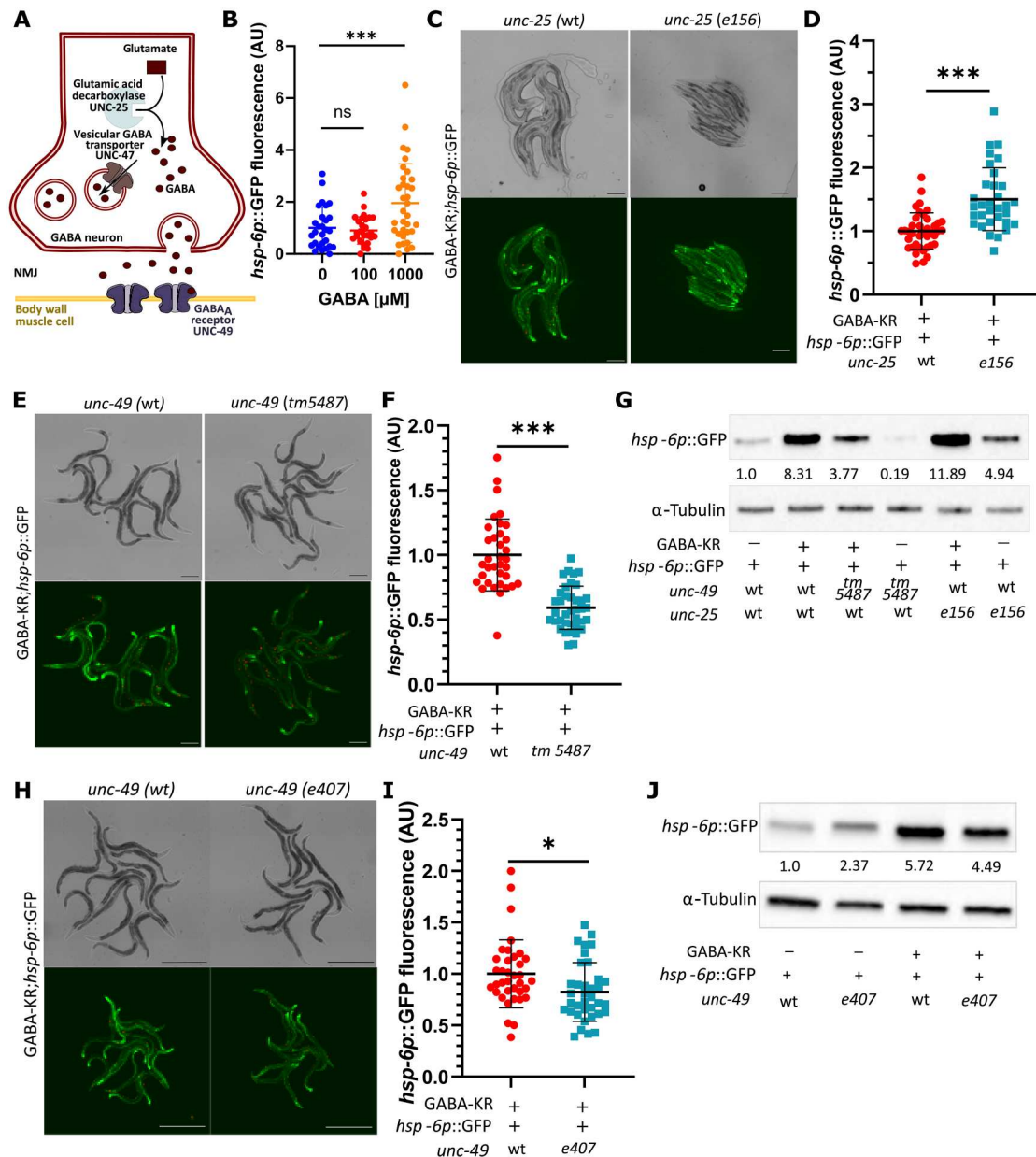


Fig. 4. GABA-KR activation of mitoUPR requires GABA_A receptor UNC-49 but is not dependent on GABA synthesis. (A) Schema of GABA production/synaptic transmission. Genes of interest: *unc-47* (GABA vesicular transporter), *unc-25* (glutamic acid decarboxylase, necessary for GABA production), and *unc-49* (inhibitory GABA_A receptor). NMJ, neuromuscular junction; GABA, γ -aminobutyric acid (90). (B) GFP fluorescence expression of *hsp-6p::GFP* reporter strains treated with 0, 100, and 1000 μ M GABA; mean \pm SD; ordinary one-way ANOVA and Dunnett's multiple comparison test, with single pooled variance; three or more biological replicates with $N \geq 6$ for each condition. (C) Fluorescent (bottom) and brightfield (top) images of *hsp-6p::GFP* expression in GABA-KR;*hsp-6p::GFP* (left) and GABA-KR;*hsp-6p::GFP*; *unc-25(e156)* (right). Scale bar, 200 μ m. (D) GFP fluorescence expression in GABA-KR;*hsp-6p::GFP* strain with WT *unc-25* or mutant *unc-25(e156)*. Unpaired *t* test; mean \pm SD; three or more biological replicates with $N \geq 6$ for each condition. (E) Fluorescent (bottom) and brightfield (top) images of *hsp-6p::GFP* expression in GABA-KR;*hsp-6p::GFP* (left) and GABA-KR;*hsp-6p::GFP*; *unc-49(tm5487)* (right). Scale bar, 200 μ m. (F) GFP fluorescence expression in GABA-KR;*hsp-6p::GFP* strain with WT *unc-49* or mutant *unc-49(tm5487)*. Unpaired *t* test; mean \pm SD; three or more biological replicates with $N \geq 6$ for each condition. (G) Western blot of *hsp-6p::GFP* expression in GABA-KR;*hsp-6p::GFP* worms in the presence of *unc-25(e156)* or *unc-49(tm5487)* with respective controls; representative of two biological replicates. (H) Fluorescent (bottom) and brightfield (top) images of *hsp-6p::GFP* in GABA-KR;*hsp-6p::GFP* (left) and GABA-KR;*hsp-6p::GFP*; *unc-49(e407)* (right). Scale bar, 500 μ m. (I) GFP fluorescence expression in GABA-KR;*hsp-6p::GFP* strain with WT *unc-49* or mutant *unc-49(e407)*. Unpaired *t* test; mean \pm SD; three or more biological replicates with $N \geq 6$ for each condition. (J) Western blot of *hsp-6p::GFP* expression in GABA-KR;*hsp-6p::GFP* worms in *unc-49(+)* and mutant *unc-49(e407)* strains; representative of two biological replicates. WBs, Western blots: Values indicate the *hsp-6p::GFP*/ α -tubulin ratios normalized to *hsp-6p::GFP*.

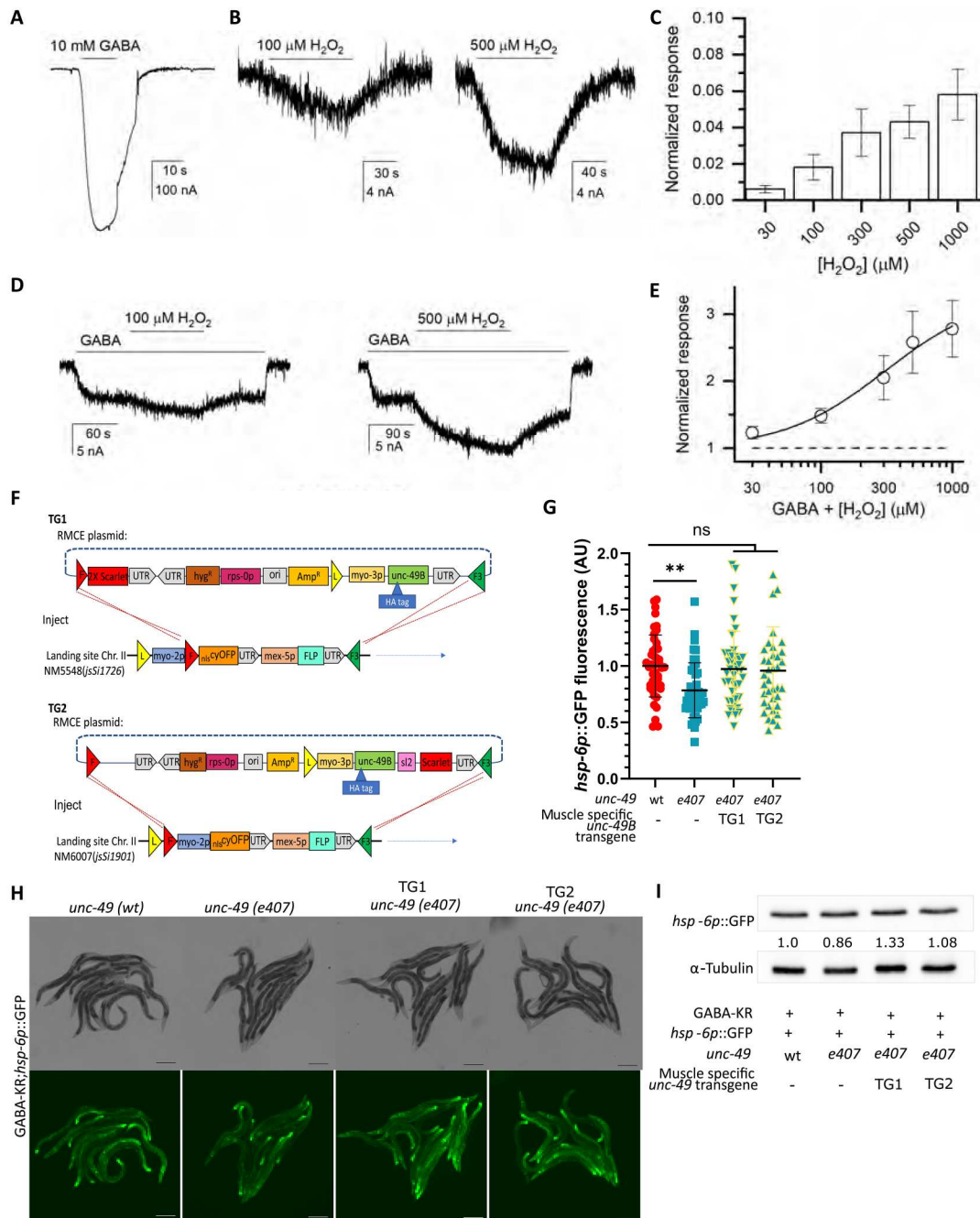


Fig. 5. H₂O₂ activates channel activity of UNC-49B. (A) Representative trace from an oocyte expressing UNC-49B exposed to 10 mM (saturating) GABA. Black line: Period of GABA exposure. (B) Representative traces from the same oocyte exposed to 100/500 μM H₂O₂. (C) Summary of H₂O₂ direct activation data; mean ± SEM (n = 5 to 9 cells/concentration) of current responses normalized to the response to 10 mM GABA in the same cell. (D) Representative traces from an oocyte expressing UNC-49B, showing H₂O₂-induced potentiation of responses to low (300 to 500 μM; EC₃) GABA. (E) H₂O₂ concentration-response relationship for potentiation of GABA-activated receptors; mean ± SEM for potentiation (1 = no effect), five cells. The curve shows a fit of pooled data to the Hill equation with an offset constrained to 1. Fitting the potentiation concentration-response curve for UNC-49 yielded a maximal response of 3.3 ± 0.6 (best-fit parameter ± SE of the fit; 1 = no effect), EC₅₀ of 311 ± 165 μM, and a Hill coefficient of 1.12 ± 0.34. (F) Transgene creation and injection for reexpression of UNC-49B in muscle cells. Colored triangles represent loxP (yellow), FRT (red), and FRT3 (green) recombinase sites. Resulting plasmids were injected into WT or *hsp-6p::GFP*;GABA-KR;*unc-49(e407)* animals with the landing site on Chr II. (G) GFP fluorescence expression in GABA-KR;*hsp-6p::GFP* strain with WT or mutant *unc-49(tm5487)* in the presence/absence of TG1/TG2. Ordinary one-way ANOVA and Dunnett's multiple comparisons test, with a single pooled variance, mean ± SD, three or more biological replicates with N ≥ 10 for each condition. (H) Fluorescent (bottom) and brightfield (top) images of *hsp-6p::GFP* expression in GABA-KR;*hsp-6p::GFP* (left) and GABA-KR;*hsp-6p::GFP*;*unc-49(tm5487)* (right). Scale bar, 200 μm. (I) Western blot of *hsp-6p::GFP* expression in GABA-KR;*hsp-6p::GFP* worms in WT and mutant *unc-49(e407)* strains and in the presence/absence of TG1/TG2; one biological replicate. Values indicate the *hsp-6p::GFP*/α-tubulin ratio normalized to GABA-KR;*hsp-6p::GFP*.

Two independent strains and transgenes were generated. The TG1 strain expressed UNC-49B and scarlet under the *myo-3* and *myo-2* promoters, respectively. TG2 expressed UNC-49B under the *myo-3* promoter with coexpression of scarlet in muscle (Fig. 5F and tables S2 to S5). Compared to the *unc-49* mutant GABA-KR;*hsp-6p::GFP;unc-49(e407)* control strain, we observed that both TG1 and TG2 significantly rescued the decrease in mitoUPR expression caused by *unc-49* mutation (Fig. 5, G and H) back to the levels of the GABA-KR;*hsp-6p::GFP*-positive control based on imaging and Western blot analysis (Fig. 5I). Hence, expression of UNC-49B in muscle cells is sufficient to rescue the mitoUPR phenotype.

GABAergic redox signaling induces vulnerability to proteostasis disease

The stress response pathways activated by low amounts of ROS in GABA neurons, including mitoUPR, SOD-3, and GST-4 (Fig. 2), are often considered to be cytoprotective and hormetic (63). We therefore hypothesized that activation of stress responses by GABA-KR would improve proteostasis-related disease phenotypes. To test this, we first used the GMC101 strain that expresses full-length human amyloid- β ($A\beta$)_{1–42} in *C. elegans* body wall muscle cells, where $A\beta$ _{1–42} can oligomerize, aggregate, and induce age-progressive paralysis at 25°C (64). This strain displays increased ROS production (65), and $A\beta$ proteotoxicity is reduced by enhanced mitochondrial proteostasis (66), suggesting that activation of the mitoUPR by GABAergic redox signaling might alleviate the disease phenotype. However, the number of paralyzed worms 12 to 24 hours after induction of proteostatic stress by temperature upshift was significantly increased in the presence of GABAergic KR under low light conditions (Fig. 6A). To test whether GABAergic redox signaling induced vulnerability to other proteostasis diseases, we next evaluated the motility phenotype of a spinocerebellar ataxia (SCA3) strain that overexpresses the aggregation-prone human ATXN3 protein in all neurons as either WT ATXN3, with 14 CAG repeats (AT3q14), or expanded ATXN3, with 75 or 130 CAG repeats (AT3q75 and AT3q130), in all *C. elegans* neurons (67). Coexpression of GABA-KR in the AT3q14 and AT3q130 strains worsened motility under light conditions (0 mW/cm²) that do not induce deleterious phenotypes or oxidative stress in GABA-KR worms (Fig. 6B) and hence seem to induce neuronal vulnerability. These studies indicate that GABAergic redox signaling induces vulnerability to proteostasis disease in neurodegenerative models.

Activation of the mitoUPR by a spinocerebellar ataxia neurodegenerative disease model requires *unc-49*

We hypothesized that GABAergic redox signaling and UNC-49 may function in proteostasis and neurodegenerative disease since cell nonautonomous activation of mitoUPR was observed in response to pan-neuronal expression of the aggregation-prone Q40 protein, an artificial polyQ tract made up of 40 glutamines (Q40) (49). In addition, altered ROS levels and redox biology are often associated with neurodegeneration, especially diseases of protein aggregation (36, 49, 68). The GABAergic system has also been shown to contribute to neurodegeneration since an SCA3 disease model expressing mutant ataxin-3 (ATXN3) with 89 CAG repeats displays increased ROS levels, decreased life span, and neurodegeneration (36).

To determine whether physiologically relevant polyQ neurodegeneration models activate the mitoUPR expression in a ROS- and UNC-49-dependent manner, we used the pan-neuronal SCA3 *C. elegans* disease model (67), since the model displays a motility defect and a polyQ length-dependent increase in protein aggregation (67), which can be alleviated with antioxidant treatment, implicating ROS in the disease etiology (37).

All three SCA3 strains (AT3q14, AT3q75, and AT3q130) displayed increased mitoUPR as assessed by *hsp-6p::GFP* expression (Fig. 6C and fig. S6A). To test whether mitoUPR activation was dependent on ROS, we treated the strains expressing AT3q14;*hsp-6p::GFP* and AT3q130;*hsp-6p::GFP* with the RSP antioxidant extract. The antioxidant extract significantly decreased mitoUPR activation in the AT3q14 and AT3q130 *hsp-6p::GFP* model (fig. S6, B and C), indicating that ROS is required to activate the mitoUPR. To determine whether the SCA3-dependent increase in mitoUPR also required *unc-49*, we crossed the more disease-relevant AT3q130 polyQ expansion model with both *unc-49* mutations (*e407* and *tm5487*). These loss-of-function *unc-49* mutations significantly decreased *hsp-6p::GFP* levels by 23% and 18% (Fig. 6, D to I), respectively. These results demonstrate that *unc-49* is required for cell nonautonomous activation of the mitoUPR by a pan-neuronal model of proteostasis disease as well as GABAergic redox signaling.

DISCUSSION

Technological advances enable tissue-specific investigation of ROS at levels ranging from redox signaling to oxidative stress

New technologies to probe the complex chemistry and biology of oxidation-reduction reactions in cells and organisms are often the rate-limiting step to conceptual advances in redox biology (69, 70). Important new tools include sensors for specific types of ROS, redox couples, and oxidized proteins (13, 70).

Optogenetic tools have revolutionized spatiotemporal control of ROS production (13, 14, 71). While these tools have primarily been used to study oxidative stress, cell ablation, or protein inhibition (e.g., CALI) (15, 17, 71), studies such as ours and others indicate that they are useful to investigate spatial aspects of redox signaling as well (18, 72). As a transparent, multicellular organism, *C. elegans* is ideally suited to provide new insights into many aspects of redox biology and signaling, especially those that are tissue-specific or are integrated across multiple tissues. *C. elegans* has many endogenous sources of ROS that are known to be functionally involved in diverse biological processes, including BLI-3, KRI-1, and GLB-12, as well as the mitochondria (2). The spatiotemporal control afforded by optogenetics is ideal to investigate how endogenous ROS mechanistically contribute to varied biological processes.

Our study advanced optogenetic approaches by enabling long-term production of ROS across a full continuum of levels from redox signaling to oxidative stress in many *C. elegans* worms and strains at the same time. Our use of low-cost LED lights is advantageous compared to more commonly used mercury bulbs, liquid light guides, or microscopy-based light delivery that can only be used to study a few worms at a time (15, 17, 72). High-throughput optogenetic platforms such as the one described here, and by others, will substantially advance research in redox biology (73). As we demonstrate in this study, precise control of ROS levels enables one to determine whether ROS promotes disease via damaging

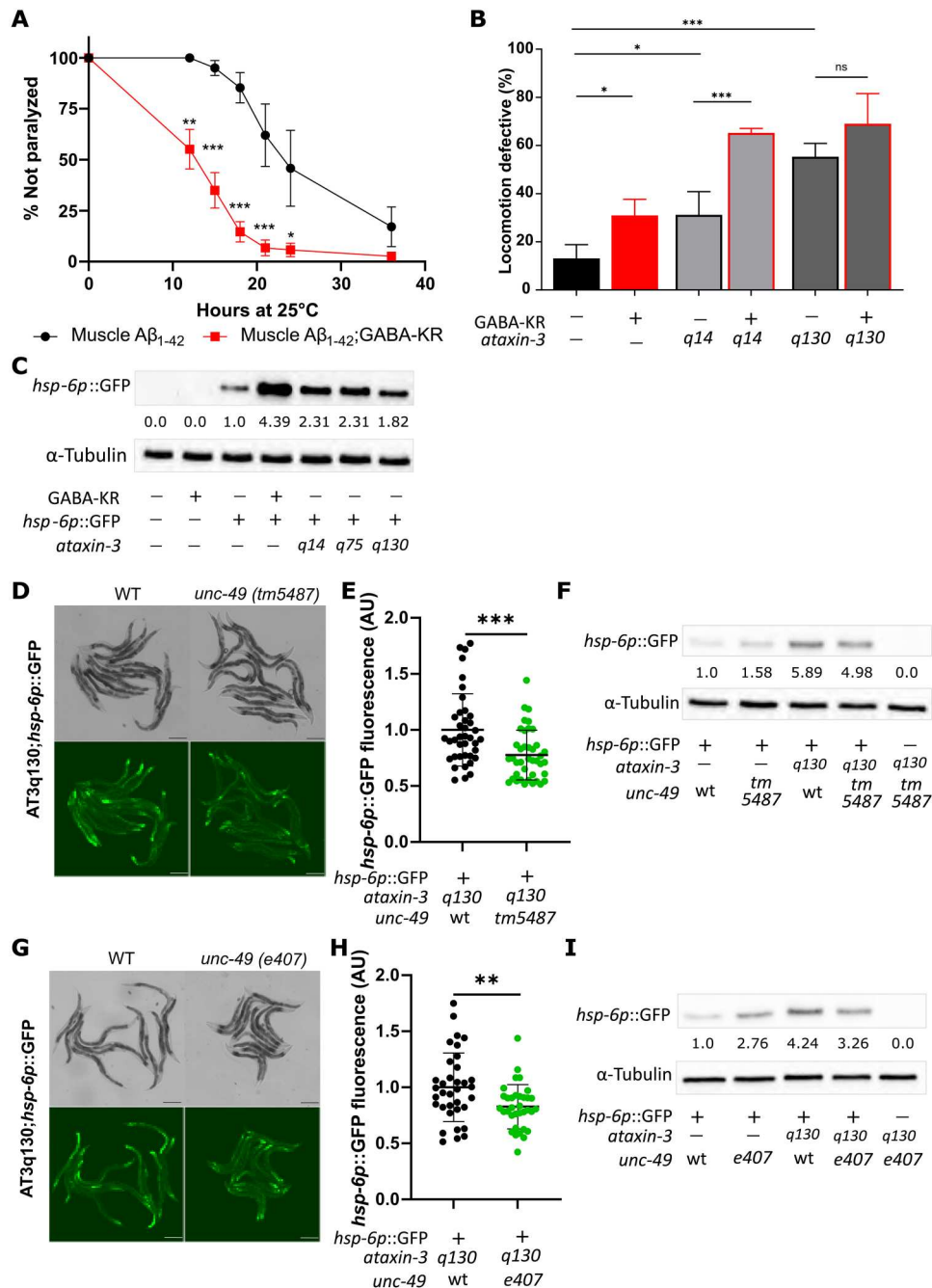


Fig. 6. SCA3 activation of mitoUPR depends on UNC-49, and GABA-KR is detrimental for neurodegeneration phenotypes. (A) Age-related paralysis phenotype in GMC101, body wall muscle $\text{A}\beta_{1-42}$ -expressing *C. elegans*. Plotted are the mean fractions of individuals not paralyzed \pm SEM, four biological replicates with $N = 45$ per experiment per strain, ordinary two-way ANOVA and Tukey's multiple comparison test, with individual variance computed for each comparison. (B) Comparison of locomotion-defective behavior of WT (blue), GABA-KR (red), and AT3q14 and AT3q130 in the absence (black) and presence (red) of GABA-KR; mean \pm SD; four biological replicates with $N \geq 38$ per experiment per strain, ordinary two-way ANOVA and Tukey's multiple comparison test, with single pooled variance. (C) Western blot analysis of *hsp-6p::GFP* expression in SCA3 AT3q14, q75, and q130 models compared to GABA-KR;*hsp-6p::GFP* and other respective controls; representative of two biological replicates. Values indicate the *hsp-6p::GFP*/ α -tubulin ratio changes normalized to the *hsp-6p::GFP* control. (D) Brightfield and fluorescent image examples of AT3q130;*hsp-6p::GFP* expression in WT and mutant *unc-49(tm5487)* strains. Scale bar, 200 μm . (E) GFP fluorescence expression in AT3q130;*hsp-6p::GFP* strain with WT or mutant *unc-49(tm5487)*; mean \pm SD, unpaired t test, three biological replicates with $N \geq 10$ per strain and replicate. (F) Western blot analysis of AT3q130;*hsp-6p::GFP* expression in the presence or absence of *unc-49(tm5487)* mutation; three biological replicates. Values indicate the *hsp-6p::GFP*/ α -tubulin ratio changes normalized to the *hsp-6p::GFP* control. (G) Brightfield and fluorescent image examples of AT3q130;*hsp-6p::GFP* expression in *unc-49(+)* and mutant *unc-49(e407)* strains. Scale bar, 200 μm . (H) GFP fluorescence expression in AT3q130;*hsp-6p::GFP* strain with *unc-49(+)* or mutant *unc-49(e407)*; mean \pm SD, unpaired t test, three biological replicates with $N \geq 10$ per strain and replicate. (I) Western blot analysis of AT3q130;*hsp-6p::GFP* expression in *unc-49(+)* and mutant *unc-49(e407)* strains; representative of three biological replicates. Values indicate the *hsp-6p::GFP*/ α -tubulin ratio changes normalized to the *hsp-6p::GFP* control.

oxidative stress versus regulation of signaling and cellular processes that can both positively and negatively regulate neuronal and organismal health (50, 74, 75).

The GABAergic system is redox-regulated

The GABAergic system regulates many organismal phenotypes associated with ROS and redox biology (33), and components of GABA neurotransmission are known to be redox regulated (23, 33–35). However, the molecular mechanisms linking GABAergic redox signaling with these downstream phenotypes are not well understood.

In this study, we demonstrate that the GABA_A receptor UNC-49 is required for the cell nonautonomous activation of the mitoUPR in response to increased ROS in GABA neurons and a pan-neuronal SCA3 proteostasis disease model. We also demonstrate that UNC-49B expression in muscle cells can rescue mutation of *unc-49*, and that UNC-49B channel activity is redox-activated by H₂O₂ in a transmitter-independent manner. While these results do not delineate which subtype of GABA neurons is involved, these results support a model of GABAergic redox signaling whereby H₂O₂ is released from GABA neurons and diffuses to muscle cells to redox-activate UNC-49 channel opening to ultimately induce the mitoUPR (Fig. 7). The pentameric ligand gated ion channel (pLGIC) superfamily, which includes GABA receptors, contributes to virtually all functions of the central nervous system (76); therefore, our discovery that redox regulation of UNC-49 increases channel activity suggests a redox mechanism explaining how H₂O₂ regulates such a diverse array of neuronal phenotypes, including addiction, neuroprotection, pain, cognition, and aging (26, 27, 77).

Redox signaling cell nonautonomously activates the mitoUPR via UNC-49

The mitoUPR has been shown to be activated by several factors in neurons including serotonin, the neuropeptide FLP-2, and Wnt/EGL-20 signaling (18, 49, 78). Our results indicate that GABAergic neurons can participate in mitoUPR as well. Notably, the mechanisms downstream of neurons that transduce cell nonautonomous activation of mitoUPR are relatively unknown besides the frizzled receptor in the intestine that is downstream of Wnt/EGL-20 signaling (49). Our results demonstrate that UNC-49 is a mediator of cell nonautonomous mitoUPR activation, and its location in muscle cells suggests that additional tissues may be involved in organism-wide coordination of this important proteostasis network. Notably, UNC-49 has previously been shown to play an important role in the cell nonautonomous regulation of intestinal immunity (32).

Our data show that the UNC-49 GABA_A receptor is also required for mitoUPR activation by the physiologically relevant model of SCA3 disease that affects all neurons, not just GABA neurons. GABA receptors and GABAergic signaling have been previously implicated in organismal proteostasis. For example, defective GABAergic signaling leads to increased aggregation of polyQ proteins in muscle cells, while GABA treatment decreased the number of polyQ aggregates (29). GABA signaling is also affected in models of Huntington's disease (HD), which have polyQ expansions in the huntingtin (htt) protein (79). However, our observation that GABAergic redox signaling induces a vulnerability to multiple proteostasis diseases models suggests that harnessing mitoUPR activation to improve this proteostasis disease may not be straightforward, but highlights GABA_A receptors as potential treatment targets.

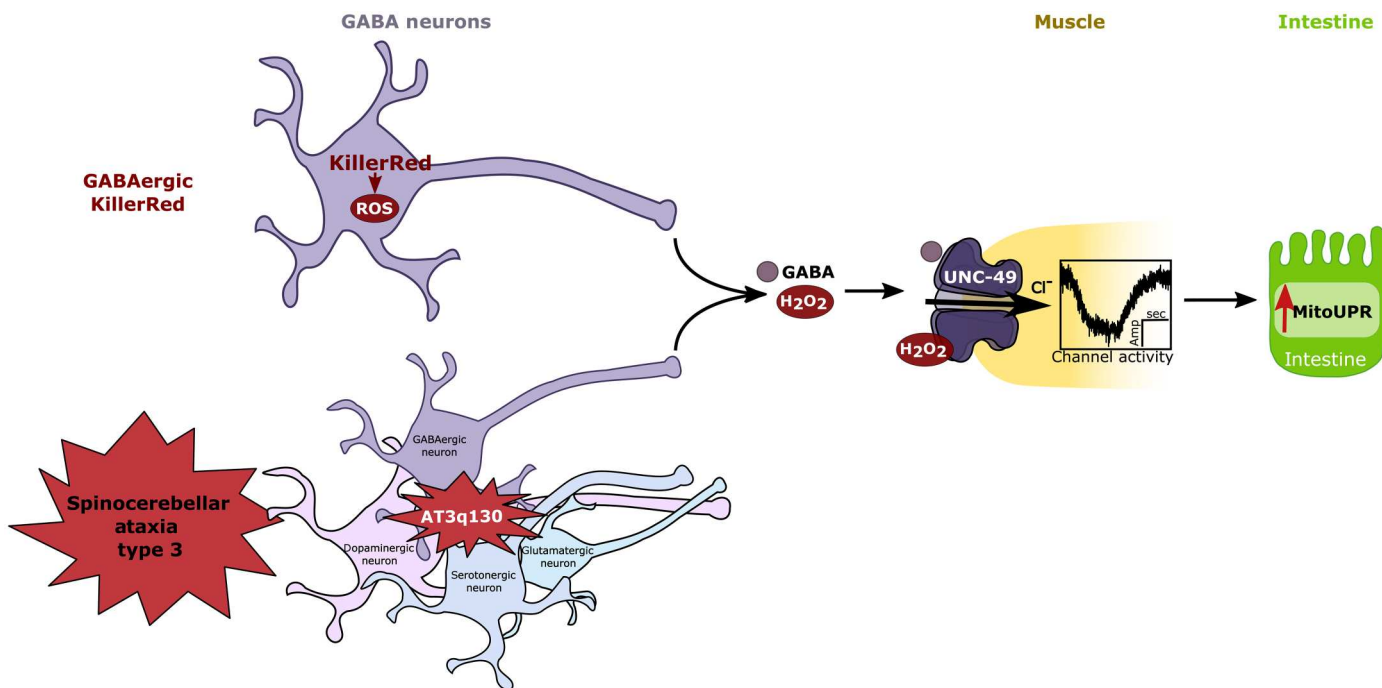


Fig. 7. Model of how GABAergic ROS and UNC-49 mediate cell nonautonomous activation of the mitoUPR in *C. elegans*. UNC-49 is required for cell nonautonomous activation of the mitoUPR in response to ROS produced in GABA neurons and neuronal ROS produced in an ataxia disease model (AT3q130). UNC-49B channel activity is sensitive to H₂O₂. These results indicate that redox activation of UNC-49 is an important mediator of redox signaling across tissues.

Last, a gap remains in understanding how GABAergic signaling is transduced downstream of UNC-49 to mitochondria in the intestine. While many studies have focused on a direct “brain-gut” connection for mitoUPR activation (18, 49, 78), our results suggest that the neuromuscular junction and muscle cells are functionally important. This is consistent with a study, demonstrating that UNC-49 mediated a neuronal-muscle connection involved in intestinal immunity (32). Further research linking redox activation of UNC-49 to mitoUPR activation in proteostasis disease provides insight into how the GABAergic system can be harnessed for therapeutic intervention.

In conclusion, GABAergic redox signaling mediates cell nonautonomous activation of several stress response pathways but also induces a vulnerability to proteostasis disease in the absence of oxidative stress. The GABA_A receptor UNC-49 is required for activation of the mitoUPR, and we demonstrate that UNC-49 channel activity is redox sensitive. Redox regulation of the GABA_A receptor may contribute to many aspects of neuronal and organismal regulation and may be targets to alleviate disease.

MATERIALS AND METHODS

Strains and general maintenance

All *C. elegans* strains were cultured and observed using standard methods (20) unless otherwise stated. *C. elegans* were maintained on NGM dishes seeded with *Escherichia coli* OP50 strain at 20°C in the dark. Strains were backcrossed to Bristol strain N2 at least five times unless otherwise stated. The GABA-KR (XE1150) and GABA-KR/GFP (XE1158) (15) strains were provided by the Hammarlund laboratory (Yale, New Haven, CT). The SCA3-related strains (AT3q14, AT3q75, and AT3q130), previously described (67), were provided by the Maciel laboratory (Universidade do Minho, ICVS, Braga, Portugal). All remaining strains were provided by the *Caenorhabditis* Genetic Center (CGC) of University of Minnesota (<https://cgc.umn.edu/>) or by the National Bioresource Project of Japan (<https://shigen.nig.ac.jp/c.elegans/top.xhtml>). Double and/or triple mutant strains were generated using common breeding techniques (80). A list of all strains used in this study, together with their abbreviations, genotypes, and sources, is provided in table S2.

Optogenetic photoactivation of GABAergic KillerRed

For photoactivation, all KillerRed strains and necessary controls were bleached to obtain developmentally synchronized egg populations (81). Between 30 and 60 eggs were transferred on evenly seeded NGM dishes (35 mm) in M9 and left to dry. Dried dishes were placed under the LED lights covered by ultraviolet (UV) and blue light filters (fig. S1). Light intensities were varied by changing the distance of the light source to the NGM dishes and by dimmers. Light intensities (0.1, 0.3, 1.0, and 3.0 mW/cm²) for each dish were measured before placement of NGM dishes. Light treatment occurred chronically for 72 hours. For dark conditions, dishes were wrapped in aluminum foil and placed under the same LED lights (light intensity, 1.0 to 3.0 mW/cm²). The temperature of the NGM dishes was measured routinely via Helect Infrared Thermometer, Non-Contact Digital Laser Temperature Gun. For experiments only done in the dark, dishes were stored in opaque boxes in the 20°C incubator.

Treatment with RSP extracts and NAC

RSP was extracted as previously described (37, 57–59) with minor modifications. Instead of the previously used automatic Soxhlet Soxtherm SE 416 (Gerhardt; Königswinter), a conventional Soxhlet extraction apparatus was used in this study. The RSP was initially extracted with petroleum ether, and the defatted RSP was dried overnight at room temperature. The second extraction of the defatted RSP was undertaken with an ethanol/water mixture (95:5), followed by one cycle of evaporation using the rotary evaporator Rotavapor R-114 (Büchi, New Castle, DE, USA). The final extract was frozen (24 hours) and free-dried (Edwards Freeze Dryer Modulyo) for 48 hours to yield the RSP extract (6.4% yield by weight).

Stock solutions of both RSP extract and NAC (Sigma-Aldrich, St. Louis, MO, USA) were prepared in M9. For NAC, the pH was adjusted with NaOH (1 M) to the same pH as M9 (pH 6.7). One hundred sixty microliters of the NAC (125 mM) and RSP (25 mg/ml) stock solutions was added to 35-mm petri dishes, filled with 4 ml of NGM and an even lawn of *E. coli* OP50 bacteria, to reach final concentrations of 5 mM (NAC) and 1 mg/ml RSP extract. Synchronized eggs of *hsp-6p::GFP* and *hsp-6p::GFP;GABA-KR* worms were transferred onto these and control dishes (M9 treatment) and cultured for 72 hours in the dark.

Assessment of stress response induction using reporter strains for *gst-4*, *sod-3*, *hsp-16.2*, *daf-16*, and *hsp-6*

Strains were grown in NGM dishes (35 mm) seeded with an even lawn of *E. coli* OP50 bacteria for 72 hours (see above). Worms were prepared for fluorescence microscopy by preparing 3% agar slides and adding a drop of levamisol (3 mM) onto the agar, and about 10 worms were added per slide. If needed, worms were oriented using an eye lash. Excess levamisol was removed, and the worms were covered with a cover slide and sealed with 3% agar. Brightfield and fluorescence images of animals were acquired using an Olympus Microscope IX70 (Figs. 1 and 2) or a Leica DMi8 (Figs. 3 to 6) using the same settings for control and light or drug-treated animals in each experiment. Fluorescence intensity of each worm was measured using Fiji (ImageJ, 1.53f51) and normalized to the respective controls. *Daf-16p::daf-16a/b::GFP* nuclear translocation was scored as nuclear or nonnuclear for each individual. The experiments were repeated at least three times independently. For the purpose of showing the results, the same level of brightness and contrast was applied to vehicle-treated animals with no impact in the fluorescence quantification of the images.

Drug toxicity assay for GABA (fig. S4A)

The toxicity of distinct concentrations of GABA in vivo was determined in the WT N2 Bristol strain, using the food clearance assay (82). The assay was performed as previously described (82, 83) in liquid culture in 96-well plate format using concentrations from 3.125 to 400 mM GABA, dissolved in deionized water. Animals treated with 5% dimethyl sulfoxide (DMSO) were used as a toxic concentration control. One independent experiment, with five wells per treatment concentration, was conducted.

Motor performance in the *C. elegans* SCA3 strain and crosses

To generate double mutants, we crossed AT3q14 and AT3q130 animals with the GABA-KR (XE1150) strain. Animals were

grown in liquid culture in 96-well format as described for the toxicity assay (see above). The motility assay was performed as previously described (37, 83), using *C. elegans* strains expressing WT ATXN3 (AT3q14) and mutant ATXN3 (AT3q130) proteins in their nervous system, along with N2 (WT) as control.

Paralysis assay

The paralysis assay was done as previously described (64) with small modifications. All strains were cultured at 20°C and developmentally synchronized via bleaching. Seventy-two hours after bleaching (time zero), individuals were shifted from 20° to 25°C and body movement was assessed after 12, 15, 18, 21, 24, and 36 hours. Worms were scored as paralyzed if they failed to complete full-body movement spontaneously or after being touch-provoked on the head. Between 45 and 55 worms were scored for each experiment per strain, and the percentage of individuals not paralyzed was calculated for each experiment ($n = 4$).

Western blots

Dishes of mixed stage, mostly adult populations, were bleached and transferred to 85-mm NGM dishes with *E. coli* OP50 bacteria as food source. After 72 hours, worms were washed off using M9 media. Each lysate sample was prepared from between 1 and 4 NGM dishes containing developmentally staged adult worms. Worms were collected in microcentrifuge tubes by gravitation and washed twice with more M9. Excess M9 was removed before freezing at -20°C . Worm lysis and Western blotting were done according to previous work (72) with minor modifications. Worm lysis was performed with the addition of equal amount of lysis buffer as worm pellet. Modified radioimmunoprecipitation assay buffer (50 mM tris-HCl, 150 mM NaCl, 20 mM EDTA, 0.5% sodium deoxycholate, 1% Triton X-100, and 0.1% SDS, pH 8.0) was used as lysis buffer combined with sonication using a sonic probe 2× for 7 s, on ice in between (amplitude 12), or in a sonic water bath with ice 10 × 30 s on/off 20 min total (amplitude 80). After centrifugation at 12,000g for 3 min at 4°C, the supernatant was collected, and protein concentration was determined by PierceBCA Protein assay (Thermo Fisher Scientific, Waltham, MA, USA). For SDS gel, samples were diluted by half with milliQ water and 5× reducing loading buffer was added. Between 15 and 20 μg of samples were then loaded onto 12% gels and separated by SDS-PAGE. Proteins were transferred to nitrocellulose membranes using Trans-Blot Turbo transfer buffer and a Trans-Blot Turbo Transfer System, and membranes were blocked in 5% bovine serum albumin (BSA) in tris-buffered saline with Tween 20 (TBST; 15.2 mM tris-HCl, 4.62 mM tris base, 150 mM NaCl, 0.5% Tween 20) for 1 hour at room temperature. Membranes were then incubated overnight at 4°C in the appropriate primary antibodies diluted 1:1000 in 5% BSA in TBST with 0.05% sodium azide: anti-KillerRed (No. AB961; Evrogen, Moscow, Russia), anti-GFP (B-2, sc-9996, Santa Cruz Biotechnology, Dallas, TX, USA), and anti- α -tubulin (DM1A, Invitrogen, Thermo Fisher Scientific, Waltham, MA, USA). After washing three times in TBST (~1 hour total), membranes were incubated in horseradish peroxidase-conjugated secondary antibodies: goat anti-mouse secondary antibody (115035-146, Jackson ImmunoResearch Laboratories Inc., West Grove, PA, USA) or goat anti-rabbit secondary antibody (111-035-144, Jackson ImmunoResearch Laboratories Inc., West Grove, PA, USA) for 1 hour at room temperature, which was followed by washing three times in TBST (~1 hour total).

Finally, proteins were visualized using ECL (Clarity Western ECL Substrate; Bio-Rad, Hercules, CA, USA) for image capture (Chem-iDoc; Bio-Rad, Hercules, CA, USA).

Receptor expression and electrophysiological recordings

The plasmid pBGR4 containing cDNA for UNC-49C (WBGene00006784, Sequence T21C12.1c) and plasmid pBGR9 containing cDNA for UNC-49F (WBGene00006784, Sequence T21C12.1f) were provided by B. Bamber (University of Toledo, Toledo, OH) (38, 39). The cDNAs for the UNC-49C and UNC-49F subunits [subcloned into vectors pBGR4 and pBGR9, respectively (39)] were linearized with Acc65I (NEB Labs, Ipswich, MA). The complementary RNAs (cRNAs) were generated from linearized cDNA using T3 mMessage mMachine (Ambion, Austin, TX, USA). Polyadenylation of RNA was carried out using Poly(A) Tailing Kit mMessage mMachine (Ambion, Austin, TX, USA).

The cDNAs encoding the UNC-49B isoform (WBGene00006784, Sequence T21C12.1b) subcloned into the T7 expression vector pBluescript II KS(+) were purchased from Bio Basic Inc. (Amherst, NY, USA). The cDNA was linearized with Acc65I. The cDNA for the human GABA_A $\rho 1$ (GenBank accession no. M62400; NM_002042) subunit in pGEMHE (84) was linearized with NheI (New England Biolabs, Ipswich, MA, USA). The cRNAs were synthesized from linearized cDNA using the mMessage mMachine T7 Ultra Transcription Kit (Ambion, Austin, TX, USA).

The UNC-49 and $\rho 1$ subunits were expressed in oocytes from *X. laevis* (African clawed frog). Quarter ovaries were purchased from Xenocyte (Dexter, MI, USA) and digested at 37°C with shaking at 150 rpm for 15 to 30 min in 2% (w/v) (mg/ml) collagenase A solution in ND96 (96 mM NaCl, 2 mM KCl, 1.8 mM CaCl₂, 1 mM MgCl₂, 5 mM HEPES; pH 7.4) with penicillin (100 U/ml) and streptomycin (100 μg/ml). Following digestion, the oocytes were rinsed in ND96 and stored in ND96 with supplements [2.5 mM Na pyruvate, penicillin (100 U/ml), streptomycin (100 μg/ml), gentamicin (50 μg/ml)] at 15°C for at least 4 hours before injections.

Oocytes were injected with 15 to 30 ng of UNC-49B cRNA, or 5 ng of UNC-49C or $\rho 1$ cRNA per oocyte. Heteromeric UNC49C/F receptors were expressed by injecting the oocytes with a total of 10 ng of cRNA in the ratio of 1:1 (UNC-49C:UNC-49F). Following injections, the oocytes were incubated at 15°C in ND96 with supplements for 1 to 3 days before conducting electrophysiological recordings.

The electrophysiological recordings were performed using standard two-electrode voltage clamp at room temperature (85, 86). The oocytes were clamped at -60 mV. Bath and drug solutions were gravity-applied from glass syringes with glass luer slips via Teflon tubing to the recording chamber (RC-1Z, Warner Instruments, Hamden, CT). The flow rate was 8 ml/min. Solutions were switched manually using four-port bulkhead switching valve and medium pressure six-port bulkhead valves (IDEX Health and Science, Rohnert Park, CA). The current responses were amplified with an OC-725C amplifier (Warner Instruments, Hamden, CT), digitized with a Digidata 1200 series digitizer (Molecular Devices, San Jose, CA), and stored using pClamp (Molecular Devices, San Jose, CA, USA). The current responses were analyzed using Clampfit (Molecular Devices, San Jose, CA, USA) to determine the peak current amplitude.

Modulation by H₂O₂ was measured by initially exposing an oocyte to a low (<5% of saturating GABA) concentration of

GABA for up to 2 min. This was followed by an application of GABA + H₂O₂ for 1 to 3 min, a wash in GABA for up to 2 min, and eventual recovery in ND96. Each cell was additionally exposed to a reference solution of a saturating concentration (10 mM) of GABA. Direct activation by H₂O₂ was tested by exposing the oocytes to 30 to 1000 μM H₂O₂. Each cell was also tested with 1 mM GABA to verify expression. Lack of effect on other targets in the oocyte membrane was verified by exposing uninjected oocytes to 300 μM H₂O₂ or 10 mM GABA. For comparison to a previous report (34), H₂O₂-mediated modulation of GABA-activated receptors was confirmed in oocytes expressing the human ρ1 GABA_A receptor.

The inorganic salts used in ND96, GABA, and H₂O₂ were purchased from Sigma-Aldrich (St. Louis, MO). The stock solution of GABA was made in ND96 at 500 mM and stored in aliquots at -20°C. H₂O₂ solution (30%, w/w) in H₂O was stored at 4°C. Dilutions were made as needed on the day of experiments.

Design of *unc-49* transgenes

unc-49 clones were created by assembling an *unc-49B* form in two parts. The common NT-terminal region (about half of the coding sequence) was created by designing a synthetic DNA fragment containing *unc-49* cDNA sequences with a hemagglutinin tag inserted between the sixth and seventh amino acid after the signal peptide sequence cleavage site and three ribosomal introns positioned at sites of native *unc-49* gene introns. The ribosomal introns were used in place of native sequences because of the concern that enhancer regions could reside in these large introns. The key aim was to assess whether muscle-specific expression of these forms was functional. The C-terminal region of the B form was synthesized with synonymous mutations that removed SapI sites.

Molecular biology

Plasmids (table S3) were constructed using Golden Gate assembly as detailed in (87). Oligonucleotides (table S4) were obtained from MilliporeSigma (Burlington, MA), and synthetic DNA fragments were purchased from Twist Biosciences (South San Francisco, CA). The structure of plasmids and transgenic insertions was confirmed using nanopore sequencing (plasmidsaurus, Eugene, OR).

Plasmid constructions (table S3)

NMp4865 pHygRR2 myo-3p *unc-49B*

The *myo-3p* from NMp4104, the *unc-49* NT and *unc-49B* CT from synthetic DNAs NMp4854 and NMp4855, and the *tbb-2* 3' untranslated region (UTR) from NMp3694 were coassembled into NMp4561 using a SapI Golden Gate assembly reaction.

NMp4866 pHygO2 myo-3p *unc-49B* *sl2* *scarlet*

The *myo-3p* from NMp4104, the *unc-49*NT and *unc-49B* CT from synthetic DNAs NMp4854 and NMp4855, the *gpd-2/-3* intergenic region from NMp4002, mScarlet from NMp4443, and the *tbb-2* 3'UTR from NMp3777 were coassembled into NMp4558 using a SapI Golden Gate assembly reaction.

Strain constructions (table S2)

jsSi1726 (NM5548) and jsSi1901 (NM6007) landing sites were introduced into JHM051 by crossing landing site males into JHM051 and backcrossing the male progeny to JHM051 and then re-homozygosing for the landing site, resulting in strains NM6388 and NM6402.

rRMCE transgenes

Plasmids were injected both into a background containing only a landing site and in a landing site; *unc-49*; *unc-25p*:killer red, *hsp-6p*::GFP background. Plasmid DNAs were injected at ~30 to 50 ng/μl. The pHygRR2-based plasmid was injected into NM5548 and NM6388, and the pHygO2-based plasmid was injected into NM6007 and NM6402 animals as described by Nonet (87). Animals were injected and cultured at 25°C. On day 3, 100 μl of hygromycin B (20 mg/ml) was added to select for insertions, and homozygous insertion-bearing animals were isolated on day 8 or day 9 after injection. Insertions were obtained for three of four conditions (three of four injections). The plasmid insertion not obtained in the mutant background was backcrossed into that background (see tables S2 and S5 for information). The insertion structure of both transgenes was confirmed by nanopore sequencing of DNA amplified from genomic DNA as described by Nonet (88).

Statistics

Statistical analyses were performed using GraphPad Prism 9 [version 9.3.1 (471)]. Continuous variables were tested for normal distribution (Shapiro-Wilk or Kolmogorov-Smirnov normality test) and outliers; they were then analyzed with *t* test, one-way or two-way analysis of variance (ANOVA), using Bonferroni's, Dunnett's, or Tukey's multiple comparison analysis for post hoc comparison. A critical value for significance of $P \leq 0.05$ was applied throughout the study. All experiments were performed at least in triplicate ($n \geq 3$), and data show mean \pm SD or mean \pm SEM unless otherwise stated. Categorical variables were analyzed using the Fisher's exact test. In all graphs, asterisks (*) are used to indicate statistical significance, with ns meaning not significant ($P > 0.05$), * $P \leq 0.05$, ** $P \leq 0.01$, and *** $P \leq 0.001$.

Supplementary Materials

This PDF file includes:

Figs. S1 to S6
Tables S1 and S2
Legends for tables S3 to S5
References

Other Supplementary Material for this manuscript includes the following:

Tables S3 to S5

REFERENCES AND NOTES

- M. Schieber, N. S. Chandel, ROS function in redox signaling and oxidative stress. *Curr. Biol.* **24**, R453–R462 (2014).
- A. Miranda-Vizuete, E. A. Veal, *Caenorhabditis elegans* as a model for understanding ROS function in physiology and disease. *Redox Biol.* **11**, 708–714 (2017).
- Y. Yang, S. M. Han, M. A. Miller, MSP hormonal control of the oocyte MAP kinase cascade and reactive oxygen species signaling. *Dev. Biol.* **342**, 96–107 (2010).
- W. A. Edens, L. Sharling, G. Cheng, R. Shapira, J. M. Kinkade, T. Lee, H. A. Edens, X. Tang, C. Sullards, D. B. Flaherty, G. M. Benian, J. David Lambeth, Tyrosine cross-linking of extracellular matrix is catalyzed by Duox, a multidomain oxidase/peroxidase with homology to the phagocyte oxidase subunit gp91phox. *J. Cell Biol.* **154**, 879–892 (2001).
- G. Li, J. Gong, H. Lei, J. Liu, X. Z. S. Xu, Promotion of behavior and neuronal function by reactive oxygen species in *C. elegans*. *Nat. Commun.* **7**, 13234 (2016).
- D. Bazopoulou, D. Knoefler, Y. Zheng, K. Ulrich, B. J. Oleson, L. Xie, M. Kim, A. Kaufmann, Y.-T. Lee, Y. Dou, Y. Chen, S. Quan, U. Jakob, Developmental ROS individualizes organismal stress resistance and lifespan. *Nature* **576**, 301–305 (2019).

7. P. Back, W. H. de Vos, G. G. Depuydt, F. Matthijssens, J. R. Vanfleteren, B. P. Braeckman, Exploring real-time in vivo redox biology of developing and aging *Caenorhabditis elegans*. *Free Radic. Biol. Med.* **52**, 850–859 (2012).
8. J. Durieux, S. Wolff, A. Dillin, The cell-non-autonomous nature of electron transport chain-mediated longevity. *Cell* **144**, 79–91 (2011).
9. D. J. Dues, C. E. Schaar, B. K. Johnson, M. J. Bowman, M. E. Winn, M. M. Senchuk, J. M. van Raamsdonk, Uncoupling of oxidative stress resistance and lifespan in long-lived isp-1 mitochondrial mutants in *Caenorhabditis elegans*. *Free Radic. Biol. Med.* **108**, 362–373 (2017).
10. C. E. Schaar, D. J. Dues, K. K. Spielbauer, E. Machiela, J. F. Cooper, M. Senchuk, S. Hekimi, J. M. van Raamsdonk, Mitochondrial and cytoplasmic ROS have opposing effects on lifespan. *PLoS Genet.* **11**, 1–24 (2015).
11. J. M. van Raamsdonk, S. Hekimi, Reactive oxygen species and aging in *Caenorhabditis elegans*: Causal or casual relationship? *Antioxid. Redox Signal.* **13**, 1911–1953 (2010).
12. M. Waghray, Z. Cui, J. C. Horowitz, I. M. Subramanian, F. J. Martinez, G. B. Toews, V. J. Thannickal, Hydrogen peroxide is a diffusible paracrine signal for the induction of epithelial cell death by activated myofibroblasts. *FASEB J.* **19**, 1–16 (2005).
13. A. P. Wojtovich, T. H. Foster, Optogenetic control of ROS production. *Redox Biol.* **2**, 368–376 (2014).
14. K. Takemoto, T. Matsuda, N. Sakai, D. Fu, M. Noda, S. Uchiyama, I. Kotera, Y. Arai, M. Horiuchi, K. Fukui, T. Ayabe, F. Inagaki, H. Suzuki, T. Nagai, SuperNova, a monomeric photosensitizing fluorescent protein for chromophore-assisted light inactivation. *Sci. Rep.* **3**, 2629 (2013).
15. D. C. Williams, R. El Bejjani, P. M. Ramirez, S. Coakley, S. A. Kim, H. Lee, Q. Wen, A. Samuel, H. Lu, M. A. Hilliard, M. Hammarlund, Rapid and permanent neuronal inactivation in vivo via subcellular generation of reactive oxygen with the use of KillerRed. *Cell Rep.* **5**, 553–563 (2013).
16. J. Kobayashi, H. Shidara, Y. Morisawa, M. Kawakami, Y. Tanahashi, K. Hotta, K. Oka, A method for selective ablation of neurons in *C. elegans* using the phototoxic fluorescent protein, KillerRed. *Neurosci. Lett.* **548**, 261–264 (2013).
17. A. P. Wojtovich, A. Y. Wei, T. A. Sherman, T. H. Foster, K. Nehrke, Chromophore-assisted light inactivation of mitochondrial electron transport chain complex II in *Caenorhabditis elegans*. *Sci. Rep.* **6**, 1–13 (2016).
18. L.-W. Shao, R. Niu, Y. Liu, Neuropeptide signals cell non-autonomous mitochondrial unfolded protein response. *Cell Res.* **26**, 1182–1196 (2016).
19. E. Yemini, T. Jucikas, L. J. Grundy, A. E. X. Brown, W. R. Schafer, A database of *Caenorhabditis elegans* behavioral phenotypes. *Nat. Method.* **10**, 877–879 (2013).
20. S. Brenner, The genetics of *Caenorhabditis elegans*. *Genetics* **77**, 71–94 (1974).
21. V. Adam-Vizi, Production of reactive oxygen species in brain mitochondria: Contribution by electron transport chain and non-electron transport chain sources. *Antioxid. Redox Signal.* **7**, 1140–1149 (2005).
22. M. E. Pamerter, Mitochondria: A multimodal hub of hypoxia tolerance. *Can. J. Zool.* **92**, 569–589 (2014).
23. M. V. Accardi, B. A. Daniels, P. M. G. E. Brown, J.-M. Fritschy, S. K. Tyagarajan, D. Bowie, Mitochondrial reactive oxygen species regulate the strength of inhibitory GABA-mediated synaptic transmission. *Nat. Commun.* **5**, 3168 (2014).
24. J. N. Cobley, M. L. Fiorello, D. M. Bailey, 13 reasons why the brain is susceptible to oxidative stress. *Redox Biol.* **15**, 490–503 (2018).
25. S. M. Kilbride, J. E. Telford, G. P. Davey, Age-related changes in H₂O₂ production and bioenergetics in rat brain synaptosomes. *Biochim. Biophys. Acta* **1777**, 783–788 (2008).
26. M. E. Rice, H₂O₂: A dynamic neuromodulator. *Neuroscientist* **17**, 389–406 (2011).
27. C. A. Massaad, E. Klann, Reactive oxygen species in the regulation of synaptic plasticity and memory. *Antioxid. Redox Signal.* **14**, 2013–2054 (2011).
28. J. W. Błaszczyk, Parkinson's disease and neurodegeneration: GABA-collapse hypothesis. *Front. Neurosci.* **10**, 269 (2016).
29. S. M. Garcia, M. O. Casanueva, M. C. Silva, M. D. Amara, R. I. Morimoto, Neuronal signaling modulates protein homeostasis in *Caenorhabditis elegans* post-synaptic muscle cells. *Genes Dev.* **21**, 3006–3016 (2007).
30. R. C. Taylor, K. M. Berendzen, A. Dillin, Systemic stress signalling: Understanding the cell non-autonomous control of proteostasis. *Nat. Rev. Mol. Cell Biol.* **15**, 211–217 (2014).
31. F. Yuan, J. Zhou, L. Xu, W. Jia, L. Chun, X. Z. S. Xu, J. Liu, GABA receptors differentially regulate life span and health span in *C. elegans* through distinct downstream mechanisms. *Phys. Ther.* **317**, C953–C963 (2019).
32. Z. Zheng, X. Zhang, J. Liu, P. He, S. Zhang, Y. Zhang, J. Gao, S. Yang, N. Kang, M. I. Afridi, S. Gao, C. Chen, H. Tu, GABAergic synapses suppress intestinal innate immunity via insulin signaling in *Caenorhabditis elegans*. *Proc. Natl. Acad. Sci. U.S.A.* **118**, e2021063118 (2021).
33. A. N. Beltrán González, M. I. López Pazos, D. J. Calvo, Reactive oxygen species in the regulation of the GABA mediated inhibitory neurotransmission. *Neuroscience* **439**, 137–145 (2020).
34. A. N. Beltrán González, J. Gasulla, D. J. Calvo, An intracellular redox sensor for reactive oxygen species at the M3-M4 linker of GABA_A1 receptors. *Br. J. Pharmacol.* **171**, 2291–2299 (2014).
35. A. Amato, C. N. Connolly, S. J. Moss, T. G. Smart, Modulation of neuronal and recombinant GABA_A receptors by redox reagents. *J. Physiol.* **517**, 35–50 (1999).
36. Y. Fardghassemi, A. Tauffenberger, S. Gosselin, J. A. Parker, Rescue of ATXN3 neuronal toxicity in *Caenorhabditis elegans* by chemical modification of endoplasmic reticulum stress. *Dis. Model. Mech.* **10**, 1465–1480 (2017).
37. F. Pohl, A. Teixeira-Castro, M. D. Costa, V. Lindsay, J. Fiúza-Fernandes, M. Goua, G. Bermanno, W. Russell, P. Maciel, P. K. T. Lin, P. Kong, T. Lin, V. Lindsay, GST-4-dependent suppression of neurodegeneration in *C. elegans* models of Parkinson's and Machado-Joseph disease by rapeseed pomace extract supplementation. *Front. Neurosci.* **13**, 1–13 (2019).
38. B. A. Bamber, R. E. Twyman, E. M. Jorgensen, Pharmacological characterization of the homomeric and heteromeric UNC-49 GABA receptors in *C. elegans*. *Br. J. Pharmacol.* **138**, 883–893 (2003).
39. B. A. Bamber, A. A. Beg, R. E. Twyman, E. M. Jorgensen, The *Caenorhabditis elegans* unc-49 locus encodes multiple subunits of a heteromultimeric GABA receptor. *J. Neurosci.* **19**, 5348–5359 (1999).
40. H. Hutter, J. Suh, GExplore 1.4: An expanded web interface for queries on *Caenorhabditis elegans* protein and gene function. *Worm* **5**, e1234659 (2016).
41. M. B. Goodman, P. Sengupta, How *Caenorhabditis elegans* senses mechanical stress, temperature, and other physical stimuli. *Genetics* **212**, 25–51 (2019).
42. S. L. Rea, D. Wu, J. R. Cypser, J. W. Vaupel, T. E. Johnson, A stress-sensitive reporter predicts longevity in isogenic populations of *Caenorhabditis elegans*. *Nat. Genet.* **37**, 894–898 (2005).
43. R. P. Brandes, F. Rezende, K. Schröder, Redox regulation beyond ROS why ROS should not be measured as often. *Circ. Res.* **123**, 326–328 (2018).
44. Y. M. Go, J. J. Gipp, R. T. Mulcahy, D. P. Jones, H₂O₂-dependent activation of GCLC-ARE4 reporter occurs by mitogen-activated protein kinase pathways without oxidation of cellular glutathione or thioredoxin-1. *J. Biol. Chem.* **279**, 5837–5845 (2004).
45. S. T. Henderson, T. E. Johnson, daf-16 integrates developmental and environmental inputs to mediate aging in the nematode *Caenorhabditis elegans*. *Curr. Biol.* **11**, 1975–1980 (2001).
46. X. X. Lin, I. Sen, G. E. Janssens, X. Zhou, B. R. Fonslow, D. Edgar, N. Stroustrup, P. Swoboda, J. R. Yates, G. Ruvkun, C. G. Riedel, DAF-16/FOXO and HLH-30/TFEB function as combinatorial transcription factors to promote stress resistance and longevity. *Nat. Commun.* **9**, 1–15 (2018).
47. J. M. van Raamsdonk, S. Hekimi, Deletion of the mitochondrial superoxide dismutase sod-2 extends lifespan in *Caenorhabditis elegans*. *PLoS Genet.* **5**, e1000361 (2009).
48. B. Leiers, A. Kampkötter, C. G. Grevelding, C. D. Link, T. E. Johnson, K. Henkle-Dührsen, A stress-responsive glutathione S-transferase confers resistance to oxidative stress in *Caenorhabditis elegans*. *Free Radic. Biol. Med.* **34**, 1405–1415 (2003).
49. K. M. Berendzen, J. Durieux, L.-W. Shao, Y. Tian, H.-E. Kim, S. Wolff, Y. Liu, A. Dillin, Neuroendocrine coordination of mitochondrial stress signaling and proteostasis. *Cell* **166**, 1553–1563.e10 (2016).
50. F. Muñoz-Carvajal, M. Sanhueza, The mitochondrial unfolded protein response: A hinge between healthy and pathological aging. *Front. Aging Neurosci.* **12**, 300 (2020).
51. D. Ganini, F. Leinisch, A. Kumar, J. J. Jiang, E. J. Tokar, C. C. Malone, R. M. Petrovich, R. P. Mason, Fluorescent proteins such as eGFP lead to catalytic oxidative stress in cells. *Redox Biol.* **12**, 462–468 (2017).
52. D. J. Kemble, G. Sun, Direct and specific inactivation of protein tyrosine kinases in the Src and FGFR families by reversible cysteine oxidation. *Proc. Natl. Acad. Sci. U.S.A.* **106**, 5070–5075 (2009).
53. Y. Liu, B. S. Samuel, P. C. Breen, G. Ruvkun, *Caenorhabditis elegans* pathways that surveil and defend mitochondria. *Nature* **508**, 406–410 (2014).
54. S. Bora, G. S. H. Vardhan, N. Deka, L. Khataniar, D. Gogoi, A. Baruah, Paraquat exposure over generation affects lifespan and reproduction through mitochondrial disruption in *C. elegans*. *Toxicology* **447**, 152632 (2021).
55. C. M. Haynes, K. Petrova, C. Benedetti, Y. Yang, D. Ron, ClpP mediates activation of a mitochondrial unfolded protein response in *C. elegans*. *Dev. Cell* **13**, 467–480 (2007).
56. G. K. Schwalfenberg, N-acetylcysteine: A review of clinical usefulness (an old drug with new tricks). *J. Nutr. Metab.* **2021**, 1–13 (2021).
57. F. Pohl, M. Goua, G. Bermanno, W. R. Russell, L. Scobbie, P. Maciel, P. Kong Thoo Lin, Revitalisation of rapeseed pomace extracts: An in vitro study into its anti-oxidant and DNA protective properties. *Food Chem.* **239**, 323–332 (2018).
58. K. Yates, F. Pohl, M. Busch, A. Mozer, L. Watters, A. Shiryaev, P. Kong Thoo Lin, Determination of sinapine in rapeseed pomace extract: Its antioxidant and acetylcholinesterase inhibition properties. *Food Chem.* **276**, 768–775 (2019).

59. F. Pohl, M. Goua, K. Yates, G. Bermano, W. R. Russell, P. Maciel, P. K. T. Lin, Impact of rapeseed pomace extract on markers of oxidative stress and DNA damage in human SH-SY5Y cells. *J. Food Biochem.* **45**, e13592 (2021).
60. S. L. McIntire, R. J. Reimer, K. Schuske, R. H. Edwards, E. M. Jorgensen, Identification and characterization of the vesicular GABA transporter. *Nature* **389**, 870–876 (1997).
61. S. Pletnev, N. G. Gurskaya, N. Pletneva, K. A. Lukyanov, D. M. Chudakov, V. I. Martynov, V. O. Popov, M. Kovalchuk, A. Wlodawer, Z. Dauter, V. Pletnev, Structural basis for phototoxicity of the genetically encoded photosensitizer KillerRed. *J. Biol. Chem.* **284**, 32028–32039 (2009).
62. WormBase WS283 March, WormBase (2022), (available at <https://wormbase.org>).
63. H. S. Yi, J. Y. Chang, M. Shong, The mitochondrial unfolded protein response and mitohormesis: A perspective on metabolic diseases. *J. Mol. Endocrinol.* **61**, R91 (2018).
64. G. McColl, B. R. Roberts, T. L. Pukala, V. B. Kenche, C. M. Roberts, C. D. Link, T. M. Ryan, C. L. Masters, K. J. Barnham, A. I. Bush, R. A. Cherny, Utility of an improved model of amyloid-beta ($A\beta$ 1–42) toxicity in *Caenorhabditis elegans* for drug screening for Alzheimer's disease. *Mol. Neurodegener.* **7**, 57 (2012).
65. X. Wang, K. Yi, Y. Zhao, Fucoidan inhibits amyloid- β -induced toxicity in transgenic *Caenorhabditis elegans* by reducing the accumulation of amyloid- β and decreasing the production of reactive oxygen species. *Food Funct.* **9**, 552–560 (2018).
66. V. Sorrentino, M. Romani, L. Mouchiroud, J. S. Beck, H. Zhang, D. D'Amico, N. Moullan, F. Potenza, A. W. Schmid, S. Rietsch, S. E. Counts, J. Auwerx, Enhancing mitochondrial proteostasis reduces amyloid- β proteotoxicity. *Nature* **552**, 187–193 (2017).
67. A. Teixeira-Castro, M. Aillon, A. Jalles, H. R. Brignull, J. L. Vilaça, N. Dias, P. Rodrigues, J. F. Oliveira, A. Neves-Carvalho, R. I. Morimoto, P. Maciel, Neuron-specific proteotoxicity of mutant ataxin-3 in *C. elegans*: Rescue by the DAF-16 and HSF-1 pathways. *Hum. Mol. Genet.* **20**, 2996–3009 (2011).
68. A. M. de Assis, J. A. M. Saute, A. Longoni, C. B. Haas, V. R. Torrez, A. W. Brochier, G. N. Souza, G. V. Furtado, T. C. Gheno, A. Russo, T. L. Monte, R. M. Castilhos, A. Schumacher-Schuh, R. D'Avila, K. C. Donis, C. R. de Mello Rieder, D. O. Souza, S. Camey, V. B. Leotti, L. B. Jardim, L. V. Portela, Peripheral oxidative stress biomarkers in spinocerebellar ataxia type 3/Machado-Joseph disease. *Front. Neurol.* **8**, 485 (2017).
69. C. C. Winterbourn, Reconciling the chemistry and biology of reactive oxygen species. *Nat. Chem. Biol.* **4**, 278–286 (2008).
70. J. M. Held, Redox systems biology: Harnessing the sentinels of the cysteine redoxome. *Antioxid. Redox Signal.* **32**, 659–676 (2020).
71. S. Xu, A. D. Chisholm, Highly efficient optogenetic cell ablation in *C. elegans* using membrane-targeted miniSOG. *Sci. Rep.* **6**, 1–13 (2016).
72. A. J. Trewin, L. L. Bahr, A. Almast, B. J. Berry, A. Y. Wei, T. H. Foster, A. P. Wojtovich, Mitochondrial reactive oxygen species generated at the complex-II matrix or intermembrane space microdomain have distinct effects on redox signaling and stress sensitivity in *Caenorhabditis elegans*. *Antioxid. Redox Signal.* **31**, 594–607 (2019).
73. I. Busack, F. Jordan, P. Sapir, H. Bringmann, The OptoGenBox—A device for long-term optogenetics in *C. elegans*. *J. Neurogenet.* **34**, 466–474 (2020).
74. S. Peña, T. Sherman, P. S. Brookes, K. Nehrke, The mitochondrial unfolded protein response protects against anoxia in *Caenorhabditis elegans*. *PLOS ONE* **11**, e0159989 (2016).
75. J. F. Cooper, E. Machiela, D. J. Dues, K. K. Spielbauer, M. M. Senchuk, J. M. van Raamsdonk, Activation of the mitochondrial unfolded protein response promotes longevity and dopamine neuron survival in Parkinson's disease models. *Sci. Rep.* **7**, 1–16 (2017).
76. Á. Nemezc, M. S. Prevost, A. Menny, P. J. Corringer, Emerging molecular mechanisms of signal transduction in pentameric ligand-gated ion channels. *Neuron* **90**, 452–470 (2016).
77. Q. Jia, D. Sieburth, Mitochondrial hydrogen peroxide positively regulates neuropeptide secretion during diet-induced activation of the oxidative stress response. *Nat. Commun.* **12**, 1–22 (2021).
78. Q. Zhang, X. Wu, P. Chen, L. Liu, N. Xin, Y. Tian, A. Dillin, The mitochondrial unfolded protein response is mediated cell-non-autonomously by retromer-dependent Wnt signaling. *Cell* **174**, 870–883.e17 (2018).
79. Y.-T. Hsu, Y.-G. Chang, Y. Chern, Insights into GABA_Aergic system alteration in Huntington's disease. *Open Biol.* **8**, 180165 (2018).
80. D. S. Fay, Classical genetic methods, in *WormBook*, The *C. elegans* Research Community, Ed. (2013), pp. 1–58.
81. T. Stiernagle, Maintenance of *C. elegans*, in *WormBook*, The *C. elegans* Research Community, Ed. (2006).
82. C. Voisine, H. Varma, N. Walker, E. A. Bates, B. R. Stockwell, A. C. Hart, Identification of potential therapeutic drugs for huntington's disease using *Caenorhabditis elegans*. *PLOS ONE* **2**, e504 (2007).
83. A. Teixeira-Castro, A. Jalles, S. Esteves, S. Kang, L. da Silva Santos, A. Silva-Fernandes, M. F. Neto, R. M. Brielmann, C. Bessa, S. Duarte-Silva, A. Miranda, S. Oliveira, A. Neves-Carvalho, J. Bessa, T. Summavielle, R. B. Silverman, P. Oliveira, R. I. Morimoto, P. Maciel, Serotonergic signalling suppresses ataxin 3 aggregation and neurotoxicity in animal models of Machado-Joseph disease. *Brain* **138**, 3221–3237 (2015).
84. P. Li, A. Khatri, J. Bracamontes, D. S. Weiss, J. H. Steinbach, G. Akk, Site-specific fluorescence reveals distinct structural changes induced in the human ρ 1 GABA receptor by inhibitory neurosteroids. *Mol. Pharmacol.* **77**, 539–546 (2010).
85. M. M. Eaton, Y. b. Lim, D. F. Covey, G. Akk, Modulation of the human ρ 1 GABA receptor by inhibitory steroids. *Psychopharmacology* **231**, 3467–3478 (2014).
86. G. Akk, D. J. Shin, A. L. Germann, J. H. Steinbach, GABA type A receptor activation in the allosteric coagonist model framework: Relationship between EC50 and basal activity. *Mol. Pharmacol.* **93**, 90–100 (2018).
87. M. L. Nonet, Rapid generation of *Caenorhabditis elegans* single-copy transgenes combining recombination-mediated cassette exchange and drug selection. *Genetics* **224**, 1–15 (2023).
88. M. L. Nonet, Efficient transgenesis in *Caenorhabditis elegans* using Flp recombinase-mediated cassette exchange. *Genetics* **215**, 903–921 (2020).
89. A. Mottis, V. Jovaisaite, J. Auwerx, The mitochondrial unfolded protein response in mammalian physiology. *Mamm. Genome* **25**, 424–433 (2014).
90. E. M. Jorgensen, GABA, in *WormBook*, The *C. elegans* Research Community, Ed. (2005).
91. N. Libina, J. R. Berman, C. Kenyon, Tissue-specific activities of *C. elegans* DAF-16 in the regulation of lifespan. *Cell* **115**, 489–502 (2003).
92. C. D. Link, J. R. Cypser, C. J. Johnson, T. E. Johnson, Direct observation of stress response in *Caenorhabditis elegans* using a reporter transgene. *Cell Stress Chaperones* **4**, 235–242 (1999).
93. T. Yoneda, C. Benedetti, F. Urano, S. G. Clark, H. P. Harding, D. Ron, Compartment-specific perturbation of protein handling activates genes encoding mitochondrial chaperones. *J. Cell Sci.* **117**, 4055–4066 (2004).
94. C. D. Link, C. J. Johnson, Reporter transgenes for study of oxidant stress in *Caenorhabditis elegans*. *Methods Enzymol.* **353**, 497–505 (2002).
95. K. Gengyo-Ando, S. Mitani, Characterization of mutations induced by ethyl methanesulfonate, UV, and trimethylpsoralen in the nematode *Caenorhabditis elegans*. *Biochem. Biophys. Res. Commun.* **269**, 64–69 (2000).
96. D. S. Fay, A. Fluet, C. J. Johnson, C. D. Link, In vivo aggregation of β -amyloid peptide variants. *J. Neurochem.* **71**, 1616–1625 (1998).

Acknowledgments: We would like to acknowledge Macintosh of Glendaveny for providing the rapeseed pomace samples for this study. We thank the *Caenorhabditis* Genetics Center (CGC; <https://cgcc.umn.edu/>), which is funded by the National Institutes of Health—Office of Research Infrastructure Programs (P40 OD010440) and the National Bioresource Project (<https://shigen.nig.ac.jp/c.elegans/>; material transfer agreement signed), for mutant nematode strains and the Maciel laboratory [Life and Health Sciences Research Institute (ICVS), School of Medicine, University of Minho, Braga, Portugal and 3ICVS/3B's—PT Government Associate Laboratory, Braga, Portugal] for the three ataxia nematode strains. The KillerRed strains were provided by the Hammarlund laboratory (Yale, New Haven, CT). We also thank B. Bamber (University of Toledo, Toledo, OH), who provided plasmid pBGR4 containing cDNA for UNC-49C and plasmid pBGR9 containing cDNA for UNC-49F. **Funding:** This publication was supported by the National Institute on Aging Awards R21 AG058037 and R21AG058037-02S1 (to K.K. and J.M.H.) and a postdoctoral fellowship from the National Ataxia Foundation (to F.P.). This work was also supported by NIH National Institute of General Medical Sciences (grant R35GM140947) and funds from the Taylor Family Institute for Innovative Psychiatric Research (to G.A.), as well as by NIH grants R56 AG072169 and RO1 AG057748 (to K.K.) by the National Institute on Aging. Grant R01GM141688 by the National Institute of General Medical Sciences supported M.L.N. **Author contributions:** F.P., G.A., M.L.N., K.K., and J.M.H. conceptualized and designed the experiments. F.P., J.M., M.L.N., and S.H. performed *C. elegans* experiments with supervision by M.L.N., K.K., and J.M.H. A.L.G. performed electrophysiology experiments under supervision by G.A. B.B. prepared the RSP extract with supervision by P.K.T.L. and K.Y. F.P., A.L.G., G.A., and J.M.H. analyzed data. F.P., A.L.G., and J.M.H. wrote the original manuscript draft with review and editing performed by all the other authors. **Competing interests:** The authors declare that they have no competing interests. **Data and materials availability:** All data needed to evaluate the conclusions in the paper are present in the paper and/or the Supplementary Materials. Most strains and plasmids can be requested from the corresponding author or the *Caenorhabditis* Genetics Center (CGC; <https://cgcc.umn.edu/>) without restrictions. The tm5487 strain can be provided by the National Bioresource Project (<https://shigen.nig.ac.jp/c.elegans/>) pending scientific review and a completed material transfer agreement.

Submitted 20 February 2023
Accepted 29 September 2023
Published 1 November 2023
10.1126/sciadv.adh2584

UNC-49 is a redox-sensitive GABA_A receptor that regulates the mitochondrial unfolded protein response cell nonautonomously

Franziska Pohl, Allison L. Germann, Jack Mao, Sydney Hou, Bayode Bakare, Paul Kong Thoo Lin, Kyari Yates, Michael L. Nonet, Gustav Akk, Kerry Kornfeld, and Jason M. Held

Sci. Adv. **9** (44), eadh2584. DOI: 10.1126/sciadv.adh2584

View the article online

<https://www.science.org/doi/10.1126/sciadv.adh2584>

Permissions

<https://www.science.org/help/reprints-and-permissions>

Use of this article is subject to the [Terms of service](#)

Science Advances (ISSN 2375-2548) is published by the American Association for the Advancement of Science. 1200 New York Avenue NW, Washington, DC 20005. The title *Science Advances* is a registered trademark of AAAS.

Copyright © 2023 The Authors, some rights reserved; exclusive licensee American Association for the Advancement of Science. No claim to original U.S. Government Works. Distributed under a Creative Commons Attribution NonCommercial License 4.0 (CC BY-NC).